Self-Constrained Baseline 3-D Correction Approach for Mobile Laser Scanning Point Cloud in Complex Urban Road Environments

Youyuan Li 🆔, Chun Liu 🆔, Hangbin Wu 🆔, and Yuanfan Qi 🆔

Abstract—Mobile laser scanning (MLS) can provide urban road spatial information, which gained increasing attention in various urban applications. However, the MLS platform position estimation is often inaccurate because the positioning observations tend to be interfered with or blocked out by surroundings in complex urban regions, resulting in the degraded quality of captured point cloud data. Instead of correcting inaccurate MLS platform positions directly, this article proposed a baseline to extract intrinsic characteristics from raw point clouds, which can be used for 3-D correction without additional reference information. Furthermore, this article designed a data-driven 3-D correction approach called self-constrained baseline correction model. First, baselines were generated from raw MLS data by extracting and connecting road markings. Next, intrinsic features information from raw data were extracted by calculating the baselines' horizontal curvature and longitudinal gradient. Then, the problematic MLS point cloud can be located by abnormal feature information of baseline accordingly, dividing raw point cloud into reference and problematic data. Finally, nonrigid correction processing was performed by building a consistent expression and iteratively minimizing the discrepancy between problematic and reference data, enhancing the accuracy consistency of the MLS road point cloud. Experiments were conducted with six typical problematic scenes collected in Shanghai, China. We demonstrated that the 2-D and 3-D average deviation of problematic data was reduced by 1.06 and 1.10 dm. The accuracy inconsistency of corrected data was also evaluated by analyzing the standard deviation of feature information. The results showed that the data quality can be improved significantly.

Index Terms—Baseline, mobile laser scanning (MLS), point cloud, 3-D correction.

I. INTRODUCTION

A. Background

WITH the rapid progress and development of urban areas, the demand for accurate 3-D information about cities, such as light detection and ranging (LiDAR) point clouds, is steadily increasing [1]. Mobile laser scanning (MLS) is an emerging technology for accurate LiDAR point clouds in urban areas [2]. An MLS system mainly comprises a data acquisition sensor (e.g., laser scanner) providing captured point cloud information and a navigation sensor [e.g., global navigation satellite system (GNSS) and inertial measurement unit (IMU)], which provides georeferencing coordinate information. The MLS system is often mounted on a moving platform (e.g., a vehicle) and can collect 3-D road information along driving paths. When a good GNSS signal is received, MLS can provide high-quality point cloud data with centimeter-level accuracy and a point density of a few thousand points/m^2, which has gained increasing attention in various urban applications, such as urban modeling [3], road infrastructure mapping [4], and autonomous vehicle driving [5].

For these practical applications, the data quality of MLS must be guaranteed. However, MLS data quality tends to degrade in a complex environment. In these complex environments, such as dense urban areas with tall buildings and street canyons, the MLS struggles to obtain good positioning results, although navigation is not completely blocked. Distortion or malposition occurs among the collected MLS point clouds. The inconsistency in data accuracy decreases the quality of MLS data in both vertical and horizontal directions, as shown in Fig. 1, where yellow and blue are MLS point clouds with different accuracies. Such inconsistency in MLS accuracy reduces data accuracy and seriously damages the structure of the road point cloud. Thus, the relative measurements of the points of interest in the point cloud cannot be guaranteed. In addition, point clouds are a very useful data type for 3-D visualization and immersive experiences [6], the degraded point cloud quality caused by inconsistency in data accuracy will affect the application of point cloud visualization.

The main cause of MLS' degraded performance is the inaccurate position estimation of the MLS platform, which is the GNSS/IMU. In dense urban areas with tall buildings and street canyons, the GNSS satellite signal is blocked by its surroundings and affected by tall buildings' multipath effect [7]. Moreover, IMU errors tend to increase very quickly over time when the navigation is of the IMU standalone solution [8], which results in a loss of accuracy and reliability of the MLS positioning trajectory. Accordingly, the MLS point cloud data quality is affected and reduced because the 3-D measurements acquired
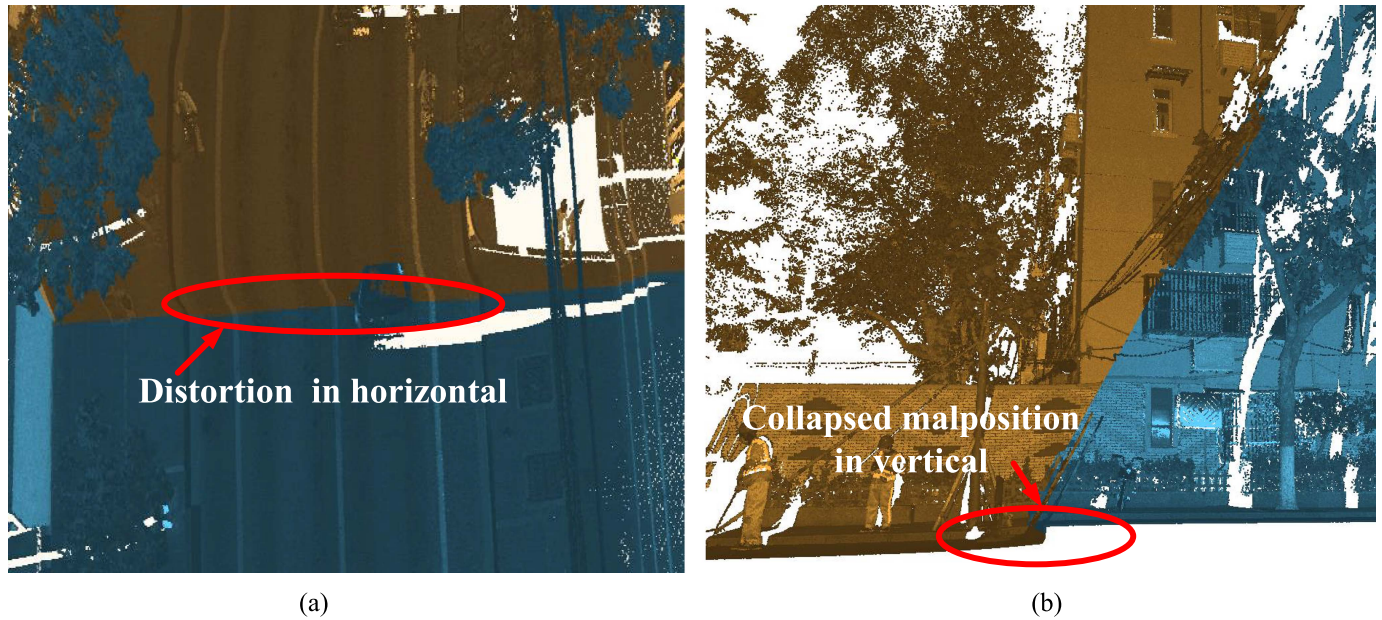
Fig. 1. Accuracy inconsistency among MLS point clouds. (a) Problematic data in horizontal. (b) Problematic data in vertical.

by the vehicle-mounted laser scanners are georeferenced to the global coordinate system based on the position data. It has been demonstrated that the shifts in the point cloud generated by MLS can reach up to meters in a complex environment [9]. Consequently, the availability and accuracy of the MLS point cloud are not always guaranteed. Unfortunately, most positioning demands are requested from urban areas, where problems frequently occur [7]. Therefore, correction solutions to improve the quality of erroneous MLS point clouds are needed, and it is essential to ensure that MLS point cloud data are corrected to the same accuracy level in a complex environment [10], [11].

The inaccurate position of the MLS platform is the major contributor to MLS' degraded performance. Unfortunately, it is difficult to improve the MLS data quality by correcting inaccurate MLS platform positions directly because the observation data for positioning the MLS platform are unstable and difficult to correct. The deviations in MLS platform positioning are often caused by various factors (such as signal block and multipath effect) in a complex environment, making establishing a general correction model intricate and arduous. More severely, the positioning observation data required for correction usually are not provided for users. This difficulty raises the challenge of improving the quality of the MLS data in a complex urban road environment.

B. Literature Review

Numerous studies have focused on enhancing MLS data quality, and the main approaches can be summarized into: ground control points (GCPs)-based technologies, model-based technologies, and data-based technologies. GCP-based technologies set GCPs along the MLS route to correct MLS data. Model-based technologies establish an MLS trajectory correction model and regenerate the MLS point cloud using an improved navigation

trajectory. Data-based technologies directly correct MLS point cloud data without MLS positioning trajectory data.

GCP-based technologies are typically used to manually survey GCPs using conventional methods to improve the quality of the MLS point cloud [12]. The raw MLS data were corrected by manually finding the corresponding target locations between the point cloud and GCPs, and then shifting the MLS point cloud position to match the surveyed GCPs. This approach can improve the trajectory position of the MLS platform and produce better overall accuracy of the corrected MLS point cloud. Local errors can be reduced, especially when errors are inconsistent within a dataset [10]. However, the procedure requires many control points (at least every 50 m), which is labor-intensive and time-consuming because it must be performed manually [9], [10], [13], [14].

Model-based technologies focus on point cloud improvement from the error sources of MLS by using raw platform positioning observations. For example, Liu et al. [11] established an MLS mathematical model, followed by a detailed analysis of the effects of the individual error source, and compensated for the poor positioning performance of the MLS trajectory in a complex environment. Han et al. [8] designed a time-variant reference transformation model to eliminate MLS positioning errors due to the loss of satellite signals. The MLS trajectory and collected point clouds can then be corrected with a few calibration points. Hussnain et al. [14] and [15] proposed an extraction method for 3-D corresponding points between the MLS point cloud and aerial images. According to them, the MLS trajectory was enhanced by integrating the corresponding points and IMU observations of the MLS platform in a complex environment. Jing et al. [10] presented an MLS trajectory correction method by combining the feature information extracted from the raw MLS point cloud. They reprocessed the navigation trajectory to produce an MLS point cloud with better quality. UAV images

[12], [16] and terrain-referenced navigation [17] were also applied to correct the MLS trajectory to improve the MLS point cloud. Although the above approaches have achieved MLS data correction by improving the MLS trajectory, the trajectory data stored independently usually are not provided as point cloud data for users, making the correction solution unavailable for relevant models [18]. Thus, the abovementioned model-based algorithms are not a universal MLS correction solution because the trajectory file is probably not given.

Comparatively, data-based technologies use data characteristics for MLS improvement, which can be directly used for MLS correction. Given that deviations often occur among MLS point clouds when the same areas are scanned several times, data-based technologies are mainly accomplished by registration between overlapping point clouds. For instance, Yu et al. [19] introduced an automatic algorithm for the global registration of MLS point clouds. Different "semantic features" scales were extracted with object detectors and selected for different iterations of an iterative closest point algorithm. Shiratori et al. [20] designed a loop-based alignment method to improve the MLS's accuracy and data quality, and loop closure was used to accurately register large numbers of dense 3-D point clouds. Yang et al. [21] developed a marker-free calibration method using an overlapped MLS point cloud to address the position inconsistency of raw MLS data, where the data features of overlapping regions were applied for the coarse-to-fine pairwise point cloud alignment. Then, the position deviations of overlapping areas were minimized to register global MLS point clouds. Data-based technologies are accomplished without any external reference or MLS trajectory data. The quality of the MLS point cloud can be improved if there is sufficient data overlap. However, current data-based correction methods require strict data acquisition conditions for overlapping, which increases the cost of the MLS data. In addition, the registration can only be matched to minimize the global differences between the two datasets, which makes it challenging to eliminate local nonrigid distortion owing to inconsistent errors within a dataset [10].

Although current approaches have achieved promising results for MLS data correction in specific scenes, these methods rely heavily on additional reference information provided by trajectory data or strict acquisition conditions. The corresponding limitation can be amplified as the amount of MLS data increases. Hence, this article attempts to determine the intrinsic characteristics of raw urban road point clouds and proposes a data-driven 3-D correction method that takes advantage of reference information from attainable data only and enhances MLS data quality in a complex environment.

II. Self-Constrained Baseline Correction Model (ScBCM)

To enhance the MLS data quality of urban road point clouds, this article attempts to make full use of intrinsic feature information among urban raw point clouds and propose a data-driven 3-D correction approach. In the practical postprocessing of the urban road MLS point cloud, we found apparent characteristics among the problematic MLS data. Even though the raw MLS point cloud has unstable data quality in a complex environment, general rules exist within some 3-D lines among the raw MLS data, as shown by the yellow lines in Fig. 2. These 3-D lines are the edges of the road markings, reflecting the 3-D distortion of the problematic urban MLS point cloud in a complex environment. It is remarkable that the road markings of the MLS point cloud with inconsistent accuracy demonstrate significant deformations, which do not conform to the code for design (such as the People's Republic of China National Standards: Road Traffic Marking GB5768.3-2009 and Technical Standard of Highway Engineering JTG B01-2014). Thus, the characteristics of road markings can reflect the MLS data quality, both vertically and horizontally, because road markings are designed without sharp swerves and surface collapse for guiding vehicles to drive in an orderly and safe manner. In addition, the characteristics of point clouds in and out of problematic urban areas should be consistent. On this basis, the portion out of the problematic urban areas can provide a corrective reference for those in the problematic urban areas. A self-constraint can be established as a correction reference without extra reference information.

Therefore, we propose a baseline for urban MLS point cloud 3-D correction. The baseline is defined as a scattered 3-D point set formed by the edge lines of road markings in the road direction, mainly composed of solid and dashed road markings.

Based on this idea, there are two main baseline functions. First, the data quality of the urban MLS point cloud, which the baseline can quantify. The horizontal curvature of the baselines can indicate the inconsistency in the accuracy of the MLS data in the horizontal direction. The problematic vertical data are reflected by the longitudinal gradient of the baselines, which can be calculated from their elevations. Therefore, the intrinsic characteristics of an urban road point cloud can be extracted to locate problematic data. The other baseline function is that, problematic data can be corrected in 3-D using the feature information of the baselines. By integrating the feature information extracted from baselines, both horizontal and vertical (horizontal curvature and longitudinal gradients), the constraint of baselines can be built to adjust the MLS data with inconsistent accuracy to the same accuracy level. Thus, we propose an urban road point cloud 3-D correction method using self-constrained baselines in a complex environment.

This article proposes a self-constrained baseline correction model (ScBCM) to improve MLS data acquired in a complex environment. ScBCM is a data-driven correction approach that takes advantage of the intrinsic feature information of urban raw point clouds. The workflow of the proposed procedure is illustrated in Fig. 3. The first step is the generation of baselines from the raw MLS data by converting 3-D points to 2-D intensity images. In the second step, we extract the intrinsic characteristics of the baseline to locate problematic MLS point clouds in a complex environment. The final step is the nonrigid correction processing of the MLS data with a consistent expression.

Two key difficulties to overcome in improving the data quality without extra reference information are extracting the intrinsic characteristics of raw MLS data and processing point clouds with data-driven nonrigid correction in a complex environment.
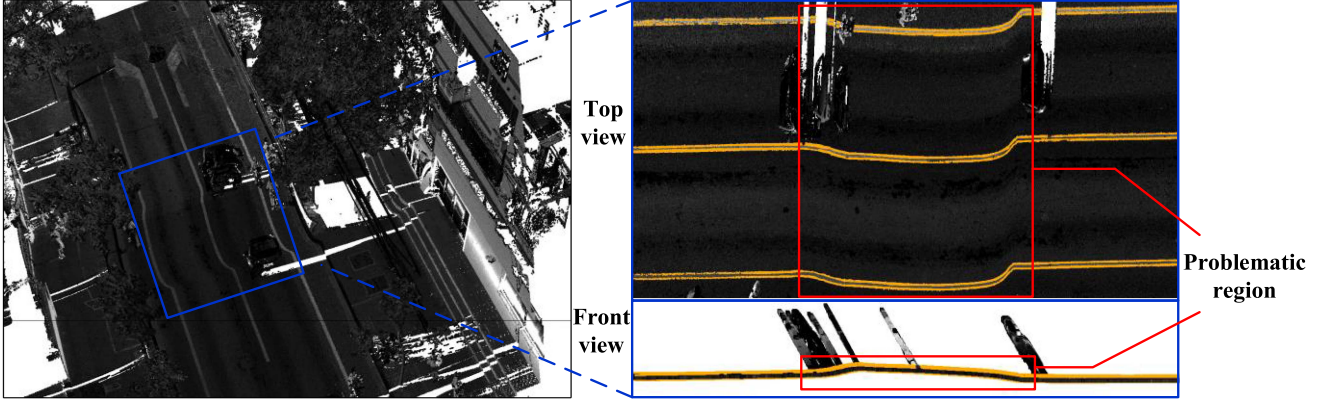
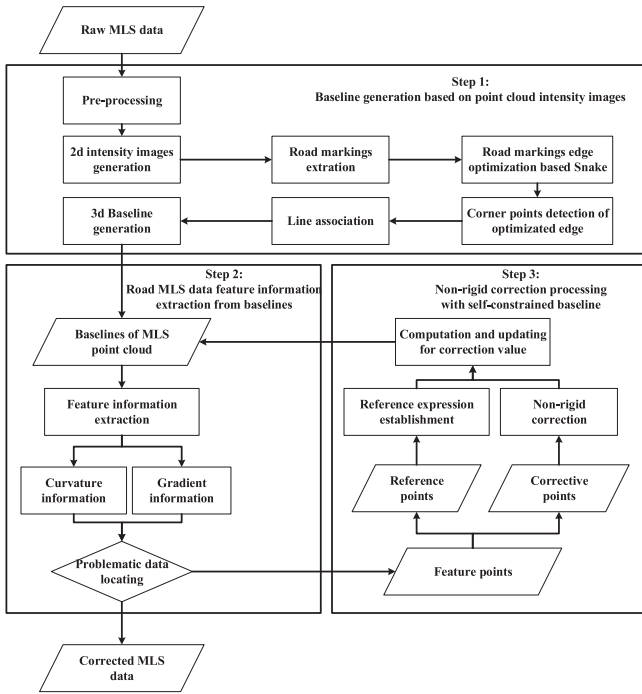Fig. 2. Baselines among problematic raw point cloud.

Fig. 3. Workflow of the proposed self-constrained baselines correction model for MLS data.

The section below will explain the computational details of the proposed model.

III. COMPUTATION OF THE PROPOSED 3-D CORRECTION MODEL

A. Baselines Generation Based on Point Cloud Intensity Images

As mentioned above, the baseline is a scattered 3-D point set formed by the edge line of the road markings in the road direction, mainly composed of solid and dashed road markings. Much information was contained in the baselines along the road mileage direction, reflecting the MLS data quality of urban roads. It is challenging to express road information directly using raw point clouds. Thus, generating accurate baselines is

critical for road information expressions and MLS data correction. Recently, many MLS studies have been conducted on road marking extraction and classification [22], [23], [24], [25], [26], [27], [28]. Owing to the large number of road-marking extraction algorithms, baseline generation is feasible and uncomplex. To generate baselines, inverse distance weighted (IDW) [29] was used to generate road intensity images, and the maximum entropy method [30] was applied for the extraction of road markings. In addition, the active contour model (snake) [31] was used for edge extraction of road markings.

Because baselines mainly comprise edge lines of road markings, identifying and extracting road markings is the basis of baseline generation. Furthermore, given that road markings are highly retroreflective materials painted on asphalt concrete pavements, the relatively high-intensity value is considered a unique characteristic for road marking extraction from raw point clouds [32].

Converting MLS point clouds into 2-D intensity images is effective for overcoming intensity and density variance issues [22]. Thus, 2-D intensity images interpreted from 3-D points are employed for MLS data with inconsistent accuracy obtained in a complex environment. First, IDW is employed to generate intensity images (grid size R is 5 cm for each pixel) from the 3-D raw point cloud, which is represented as follows:

$$d_k^2 = \left(X_k - \left(X_{\min} + \frac{(2M-1)R}{2} \right) \right)^2$$
$$+ \left(Y_k - \left(Y_{\min} + \frac{(2N-1)R}{2} \right) \right)^2 \quad (1)$$

$$I_{(M,N)} = \frac{\sum_{k=1}^{n} W_k I_k}{\sum_{k=1}^{n} W_k} \quad (2)$$

where $I_{(M,N)}$ denotes the gray value of the grid (M, N) interpolated by IDW, $W_k = \frac{1}{d_k^2}$ denotes the weight of the kth point within the grid, and n is the number of points in a grid.

Subsequently, the max entropy method [30] was applied for image binarization. The binarization threshold k was determined
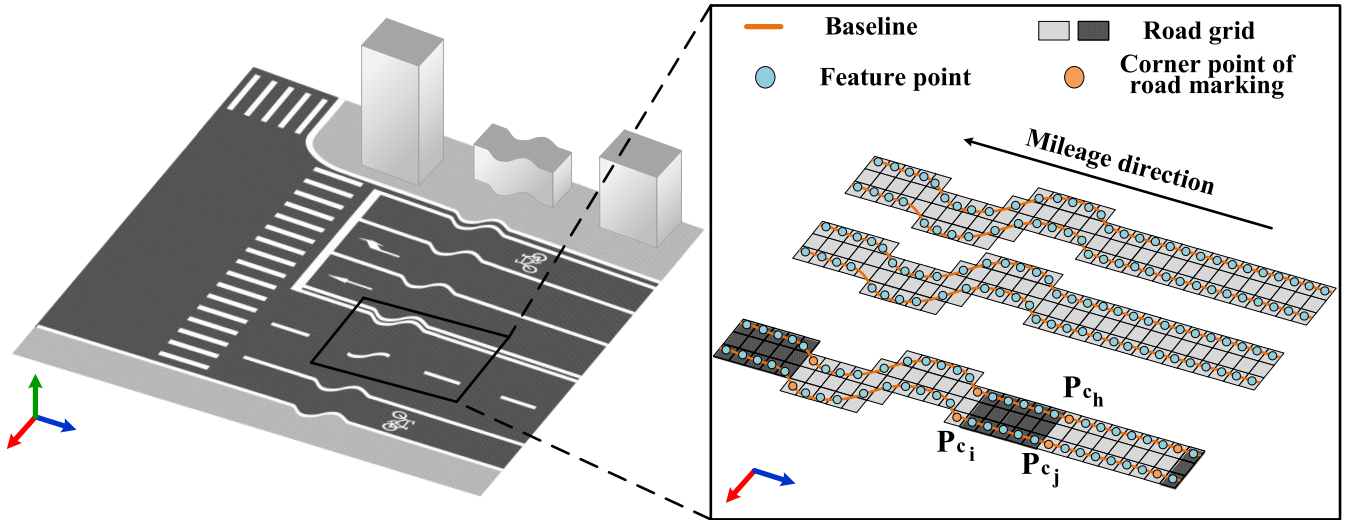
Fig. 4. Graphical illustration of the line association procedure for baseline generation.

as follows:

$$k = \max_t \left(-\sum_{i=0}^{t} \frac{P_i}{P_n} \log \frac{P_i}{P_n} - \sum_{i=t+1}^{255} \frac{P_i}{1-P_n} \log \frac{P_i}{1-P_n} \right) \tag{3}$$

$$P_n = \sum_{i=0}^{t} P_i \tag{4}$$

where P_i represents the probability of pixel gray value i.

After image binarization, the road-marking region was identified from the background. Then, connected component analysis was employed for road marking segmentation, and road marking regions of solid and dashed road markings were saved according to semantic knowledge (e.g., shape and size) [29]. Next, the Sobel edge detection algorithm was used for the edge detection of separated road markings. However, void or disconnected lane markings would affect edge detection. A snake is used to solve the problem, the snake is an energy-minimizing spline guided by external constraint forces and influenced by image forces that pull it toward features, such as lines and edges, which can be expressed as follows:

$$E_{\text{snake}}^* = \int_0^1 \left[E_{\text{int}}(v(s)) + E_{\text{image}}(v(s)) + E_{\text{con}}(v(s)) \right] ds \tag{5}$$

where E_{int} denotes the internal energy of the spline due to bending; E_{image} gives rise to the image forces; E_{con} represents the rise to the external constraint forces, and $v(s) = (x(s), y(s))$ is the position of the snake.

The edge of the extracted road markings may be discrete as segments because of dashed road markings. Line association is crucial in generating baselines by linking the discrete corners of road marking edges that topologically lie in the same lane. First, the Harris corner detector yields corner points for each road marking segment, as shown in orange in Fig. 4. Each road marking segment is divided by corner points into four parts, and the two extended parts (approximately along the milage

direction) are saved as baseline segments for baseline generation. An association process is then performed to determine the corners connected based on the orientation and distance. For each connected corner point, the orientations θ and distance ρ are computed as follows:

$$\rho = \sqrt{(X_j - X_i)^2 + (Y_j - Y_i)^2} \tag{6}$$

$$\theta = \arccos \frac{(X_j - X_i, Y_j - Y_i) \cdot \boldsymbol{v}}{\rho} \tag{7}$$

where $P_{c_j}(X_j, Y_j)$ and $P_{c_i}(X_i, Y_i)$ are two corner points distributed on different baseline segments, and $\boldsymbol{v}$ is a unit vector representing the mileage direction along the road. In the case of point P_{c_j}, point P_{c_h} with the minimal distance ρ from P_{c_j} is first removed, because point P_{c_h} and point P_{c_j} are not on the same side of the road marking. Then, the point P_{c_i} is determined and linked to point P_{c_j}, because both of distance ρ and orientation θ between P_{c_i} and P_{c_j} is minimal.

The two candidate corner points of the road-marking edge satisfying the above condition are connected, and the baseline segments of each candidate corner point are integrated into the same segment. Thus, baselines were generated by integrating the baseline segments and road points on the line of the two candidate corner points. Fig. 4 shows a graphical illustration of the line association procedure with the corner points of road markings. Finally, the 3-D laser points of the baseline can be extracted from the 2-D intensity images. In practice, the image resolution can be increased or manually adjusted to avoid "jagged" and obtain more accurate baseline 3-D points, thereby reducing the processing efficiency of ScBCM.

B. Road MLS Data Feature Information Extraction From Baselines

After generating the baselines, the feature information of the road point cloud should be extracted to reflect the MLS data quality. Accurately extracting road feature information is key to improving the quality of MLS point cloud data. Horizontal
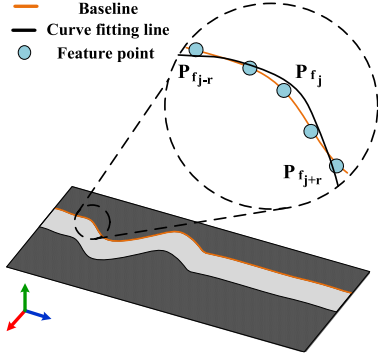
Fig. 5. Graphical illustration of curvature and gradient at P_{f_j}.

curvature (from now on referred to as curvature) and longitudinal gradient (from now on referred to as gradient) are the major geometric elements of urban roads [33]. Therefore, curvature and gradient are essential feature information for road data analysis, which can be used to express the MLS data quality. In a complex environment, the instability of MLS positioning accuracy will distort the point cloud in 3-D, causing the road baselines to show abnormally high local curvature or gradient values. According to the characteristics of problematic road clouds, the MLS data with accuracy inconsistency can be located using the feature information of the baselines. Thus, for each baseline composed of feature points $\{(x_{f_0}, y_{f_0}, z_{f_0}), (x_{f_1}, y_{f_1}, z_{f_1}), \ldots, (x_{f_i}, y_{f_i}, z_{f_i})\}$, $F(x, y)$ and $G(x, y, z)$ are designed to extract the feature information of each baseline horizontally and vertically.

As for problematic data reflected in the horizontal direction, the baseline curvature is calculated to locate the horizontal deformation. Because the baselines comprise discrete feature points, their curvature information cannot be acquired directly. Therefore, the curvature was calculated by local polynomial curve fitting (i.e., quadratic polynomial), as shown in Fig. 5. The fitting curve at the feature point $P_{f_j}(x_{f_j}, y_{f_j}, z_{f_j})$ of the baselines can be expressed as

$$\varphi_2(x) = a_3 x^2 + a_2 x^1 + a_1 = y \tag{8}$$

where $a_i(i = 1, 2, 3)$ denote the polynomial parameter and can be determined by the local feature points in the neighborhood (radius $r = 0.5$ m) of P_{f_j}.

The baseline curvature k_{f_j} at feature point $P_{f_j}(x_{f_j}, y_{f_j}, z_{f_j})$ can be formulated as

$$k_{f_j} = \frac{|2a_3|}{\left(1 + (2a_3 x_{f_j} + a_2)^2\right)^{\frac{3}{2}}}. \tag{9}$$

The longitudinal gradient is the elevation rate with respect to the distance in the direction of travel flow [34]. Therefore, the gradient of baselines can be used to locate problematic data with accuracy inconsistency in the vertical direction. The baseline gradient s_{fj} at feature point $P_{f_j}(x_{f_j}, y_{f_j}, z_{f_j})$ can be formulated as follows:

$$s_{fj} = \frac{\left|z_{f_{j-r}} - z_{f_{j+r}}\right|}{\sqrt{\left(y_{f_{j-r}} - y_{f_{j+r}}\right)^2 + \left(x_{f_{j-r}} - x_{f_{j+r}}\right)^2}} \tag{10}$$

where $P_{f_{j+r}}(x_{f_{j+r}}, y_{f_{j+r}}, z_{f_{j+r}})$ and $P_{f_{j-r}}(x_{f_{j-r}}, y_{f_{j-r}}, z_{f_{j-r}})$ denote the points with the maximum and minimum time differences of point P_{f_j}, respectively, in the neighborhood.

Before 3-D correction processing, problematic MLS data should be located according to the extracted feature information. Considering that the curvature and gradient of feature points are abnormally high in the problematic MLS data (accuracy inconsistency), the curvature threshold k_0 and gradient threshold s_0 are predefined for locating problematic data, and $\psi(F, G)$ is designed for locating problematic data, if the curvature k_{f_j} and gradient s_{f_j} of feature point P_{f_j} comply with the comprehensive threshold $\{(k_{f_j} < k_0) \wedge (s_{f_j} < s_0)\}$, the feature point P_{f_j} is saved as a reference point, which is used for reference line computation. Otherwise, P_{f_j} is saved as a corrective point, which is used for self-constrained correction.

As illustrated in Fig. 6, the baseline's spatial position is shown in the upper part of Fig. 6, and the overall feature information of the baseline is shown below. The orange dotted lines in Fig. 6(a) and (b) represent the curvature threshold k_0 and gradient threshold s_0, respectively. The first and last feature points failing to comply with the comprehensive threshold are marked with red circles in Fig. 6, corresponding to the problematic points on the baseline. Therefore, problematic points can be located successfully according to $\psi(F, G)$.

Some problematic points may be too subtle to be detected, such as the feature point at a local mileage of 50 m in Fig. 6. Thus, we extended the problematic field length along the mileage direction to l_c, which ensured all problematic feature points were included in the corrective points. Consequently, some feature points can be correctly classified as corrective points, even though the feature information appears abnormal. After the extending processing, the join points of the nonproblematic region and extended problematic field are P_s and P_e. They denote the feature point just before the problem starts and the feature point just after the problem ends, respectively, which will be used for nonrigid 3-D correction in Section III-C.

The location of problematic data is designed based on the assumption that the accuracy inconsistency is reflected by the abnormally high curvature and high gradient of the baselines. However, it is recognized that a high curvature value or high gradient value of a single baseline does not fully represent the accuracy inconsistency owing to traffic diversion lines, road patches, and road markings painted incorrectly. Therefore, the optimized scheme $\psi(F, G)$ is employed, which determines the inconsistency in accuracy when all baselines fail to comply with the comprehensive threshold at that period, such as Fig. 7(a). As shown in the red dotted box in Fig. 7(b), there is only one generated baseline failure to comply with the comprehensive threshold, which is not determined to be inconsistent in accuracy according to the optimized scheme. The optimized scheme $\psi(F, G)$ avoids incorrectly locating the correct MLS data and allows for an exceptional baseline case.

This generated baseline information will be integrated into the nonrigid correction processing in the next section, which improves the accuracy and consistency among problematic MLS data captured in a complex environment.
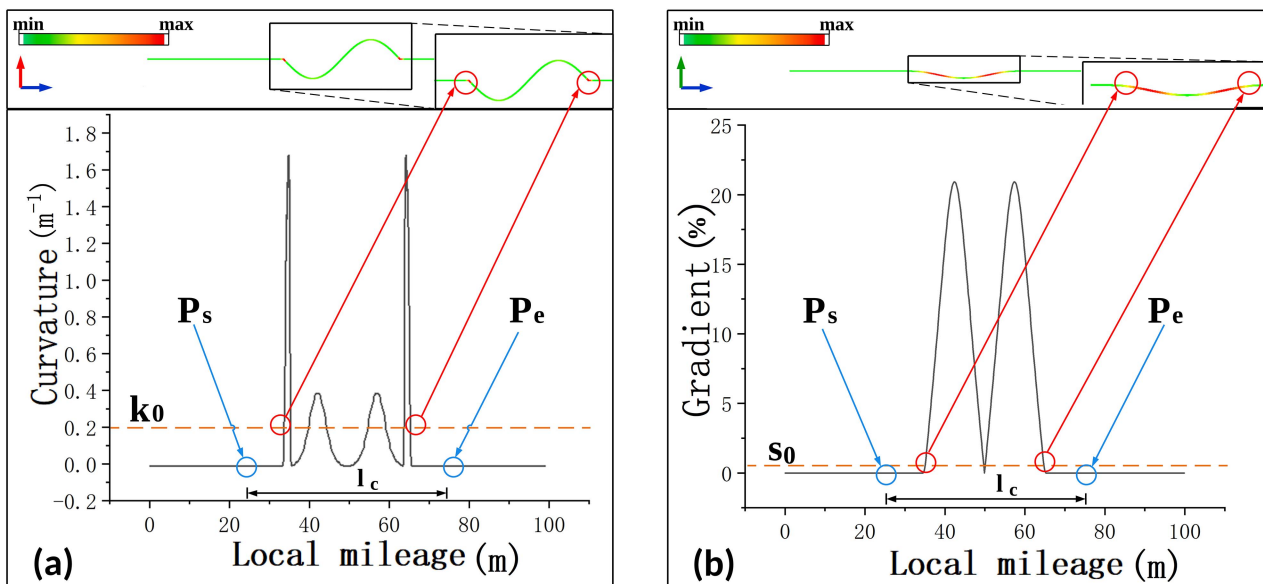
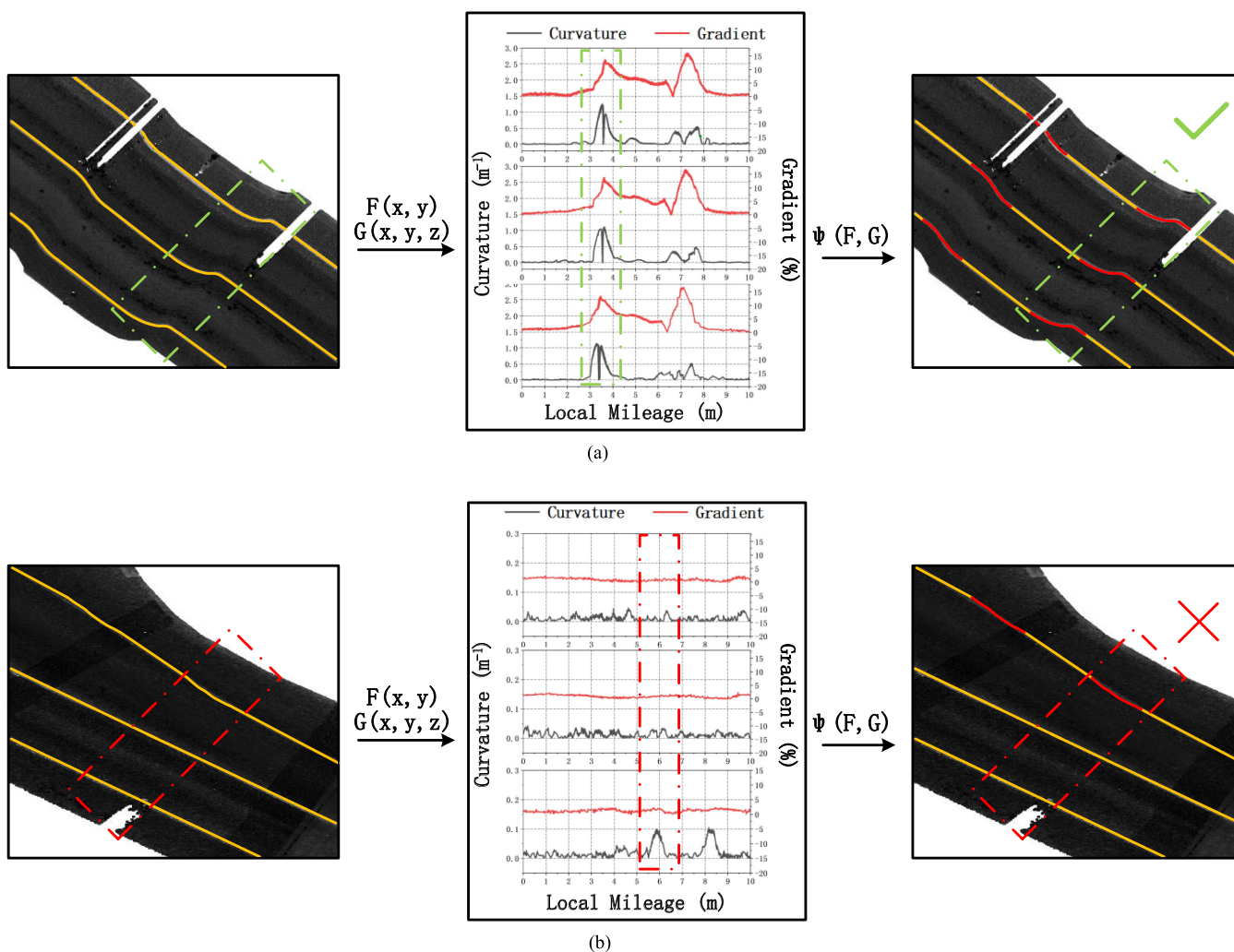Fig. 6.   Graphical illustration for locating problematic data from baselines.

Fig. 7.   (a) Positive example of problematic data locating using baseline feature information. (b) Negative example of problematic data locating using baseline feature information.
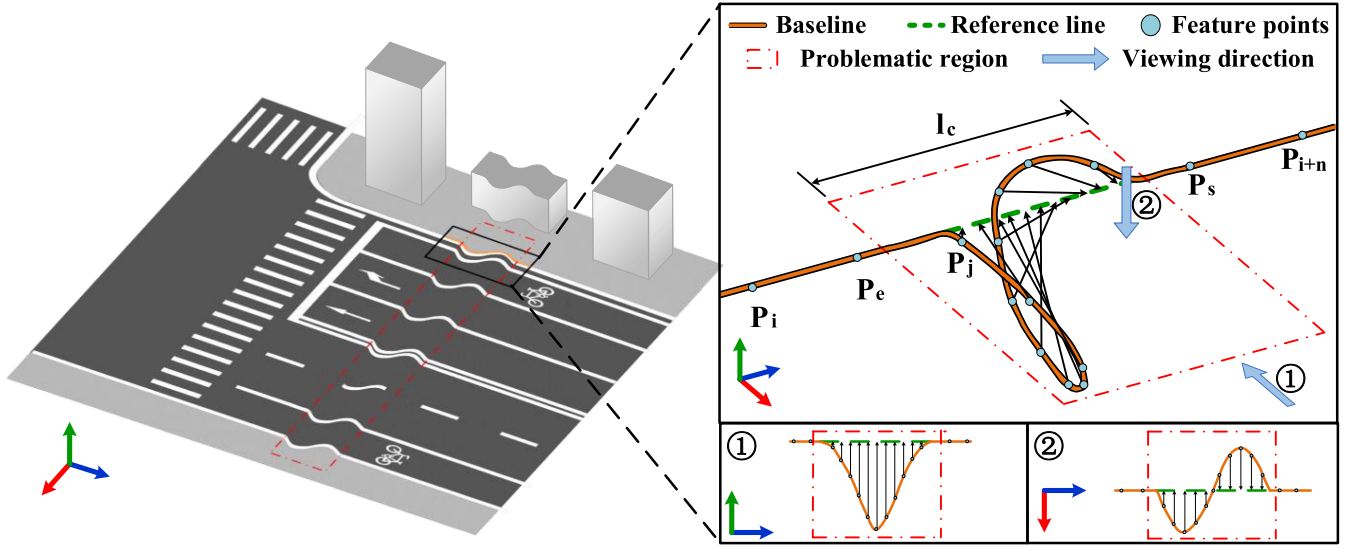
Fig. 8. Graphical illustration of nonrigid 3-D correction.

C. Nonrigid 3-D Correction Processing With Self-Constrained Baseline

Nonrigid correction processing is the core process of ScBCM, which plays a crucial role in MLS point cloud improvement in a complex environment. As shown in Fig. 2, there is nonrigid deformation and distortion among the point clouds captured in a complex environment due to the instability of the GNSS position signal and the nonlinear behavior of the INS position errors. Thus, nonrigid correction processing is designed for MLS data in a complex environment, and $\{x, y, z, \text{intensity}, \text{acquisition time}\}$ information on the point cloud are used for this section.

As outlined in Section III-B, the inconsistency in the accuracy of the captured MLS point cloud is located when the curvature or gradient of the baselines is abnormally high. The feature information of the baselines divides the feature points into reference and corrective points, which are distributed in different regions. As shown in Fig. 8, the accuracy inconsistency problem occurs in the region (dotted box) over which the MLS vehicle is driven in the acquisition time of the corrective points. The lower right illustration of Fig. 8 is the front view ① and top view② of the baseline. The region before and after the problem occurs denotes the area where MLS data are captured in the acquisition time of the reference points. As mentioned in Section III-B, the feature points in the extended field (the field length along the mileage is expressed as l_c in Fig. 8) are considered problematic data and are used for nonrigid correction. According to the above information, nonrigid correction processing is described as follows:

As discussed above, the data quality of the MLS point cloud is reflected by the baselines. For MLS data without inconsistencies, the extracted feature points of the baselines should remain stable and consistent in accuracy. Each baseline among the MLS data with consistent accuracy can establish a consistent expression (the direction of which is extremely close to the road direction) using feature points on the baselines. Therefore, to ensure that the point cloud is corrected to the same level of accuracy, the feature points on the baselines must match a consistent baseline expression. For baselines with inconsistencies in accuracy, the feature points are divided into corrective and reference points, as mentioned in Section III-B. Because reference points are considered reliable in the region before and after the problem occurs, a reference expression of the baseline with consistent accuracy can be established by reference points. The reference expression is shown as the reference line in Fig. 8.

For baseline consistency, the reference points on the baseline must constrain the corrective points. The self-constraint for baselines is built to control the corrective points on the baseline to match the reference expression established by the reference points on the baseline. Thus, the accuracy of the baselines was consistent under the principle of self-constraint.

According to the Technical Standard of Highway Engineering JTG B01-2014 in China, urban roads and road markings are designed as straight lines, circular curves, and transitional curves. Therefore, to get closer to the designed form of urban roads, we used a kth degree polynomial for the reference line to adapt to straight and curved roads. The reference line is the expression of the reference points on the baselines, which can be expressed by a polynomial of degree k

$$\begin{cases} \varphi_k\ (x) = \ y = a_{k+1}\ x^k + a_k x^{k-1} + \cdots + a_1 \\ \omega_k\ (x) = \ z = b_{k+1}\ x^k + b_k x^{k-1} + \cdots + b_1 \\ \qquad \varphi_k\ (x_s) = y_s \\ \qquad \varphi_k\ (x_e) = y_e \\ \qquad \omega_k\ (x_s) = z_s \\ \qquad \omega_k\ (x_e) = z_e \end{cases} \tag{11}$$

where $\mathrm{P}_s(x_s, y_s, z_s)$ and $\mathrm{P}_e(x_e, y_e, z_e)$ denote the feature point just before the problem starts and immediately after the problem ends, respectively.

The reference points $\mathrm{P}_i(x_i, y_i, z_i)$ can determine the reference line in the region before and after the problem occurs,

which can be formulated as follows:

$$\left\{ \begin{array}{l} \begin{pmatrix} V_y \\ V_z \end{pmatrix} = \begin{pmatrix} x_i^k & x_i^{k-1} & \cdots & 1 & 0 & 0 & \cdots & 0 \\ 0 & 0 & \cdots & 0 & x_i^k & x_i^{k-1} & \cdots & 1 \end{pmatrix} \begin{pmatrix} a_{k+1} \\ a_k \\ \vdots \\ a_1 \\ b_{k+1} \\ b_k \\ \vdots \\ b_1 \end{pmatrix} - \begin{pmatrix} y_i \\ z_i \end{pmatrix} \\[5em] \begin{pmatrix} x_s^k & x_s^{k-1} & \cdots & 1 & 0 & 0 & \cdots & 0 \\ x_e^k & x_e^{k-1} & \cdots & 1 & 0 & 0 & \cdots & 0 \\ 0 & 0 & \cdots & 0 & x_s^k & x_s^{k-1} & \cdots & 1 \\ 0 & 0 & \cdots & 0 & x_e^2 & x_e^{k-1} & \cdots & 1 \end{pmatrix} \begin{pmatrix} a_{k+1} \\ a_k \\ \vdots \\ a_1 \\ b_{k+1} \\ b_k \\ \vdots \\ b_1 \end{pmatrix} + \begin{pmatrix} -y_s \\ -y_e \\ -z_s \\ -z_e \end{pmatrix} = 0. \end{array} \right. \tag{12}$$

The standard matrix form is given

$$\left\{ \begin{array}{l} V = B\hat{X} - L \\ C\hat{X} + W_x = 0. \end{array} \right. \tag{13}$$

The polynomial parameter of the reference line can be

$$\hat{X} = \left(N^{-1} - N^{-1} C^T N_c^{-1} C N^{-1} \right) W - N^{-1} C^T N_c^{-1} W_x \tag{14}$$

where $N_c = C N^{-1} C^T$, $N = B^T B$, and $W = B^T L$.

Nonrigid correction can be expressed as follows:

$$\left\{ \begin{array}{l} (x_e - x_s)\, x + (y_e - y_s)\, y + (z_e - z_s)\, z \\ \quad - (x_e - x_s)\, x_j - (y_e - y_s)\, y_j - (z_e - z_s)\, z_j = 0 \\ y = a_{k+1}\, x^k + a_k x^{k-1} + \cdots + a_1 \\ z = b_{k+1}\, x^k + b_k x^{k-1} + \cdots + b_1 \\ x_e < x < x_s \end{array} \right. \tag{15}$$

where $P_j(x_j, y_j, z_j)$ is corrective point in the region where the problem occurs. Correspondingly, the nonrigid corrected $P'_j(x'_j, y'_j, z'_j)$ can be determined by (15).

The correction value (Vx_{jj}, Vy_j, Vz_j) of feature point P_j can be obtained as follows:

$$\left\{ \begin{array}{l} Vx_j = x'_j - x_j \\ Vy_j = y'_j - y_j \\ Vz_j = z'_j - z_j. \end{array} \right. \tag{16}$$

Subsequently, the MLS point cloud can be corrected as follows:

$$\left\{ \begin{array}{l} X'_{(t)} = X_{(t)} + Vx_{(t)} \\ Y'_{(t)} = Y_{(t)} + Vy_{(t)} \\ Z'_{(t)} = Z_{(t)} + Vz_{(t)} \end{array} \right. \tag{17}$$

where $(Vx_{(t)}, Vy_{(t)}, Vz_{(t)})$ denotes the correction value obtained by feature point, which is collected at time t. $P_{(t)}$ and $P'_{(t)}$ are MLS points before and after correction, respectively. In terms of a problematic scene, multiple baselines can be extracted to use for the proposed correction model, each baseline can provide

a correction value, and thus, the average value of each baseline at the same acquisition time is used for the MLS laser point accordingly.

Subsequently, the corrected feature points of the baselines are obtained in the problematic region, and the correction value of the new baselines is updated. Section III-B was repeated until each feature point of the baseline complied with the comprehensive threshold. By the iterations described in Section III-B, a 3-D updated correction value can be determined and used to correct the MLS point cloud data of the area where accuracy inconsistency occurs. Finally, corrected MLS point cloud data can be generated using ScBCM correction.

IV. CASE STUDY

To verify the effectiveness of the proposed method, a series of experiments were carried out on MLS datasets. Next, the experimental data and parameter settings are described in detail. The experimental results of the proposed approach are presented at the end of this section.

A. Data Description of Experimental Scenes

The MLS point cloud data were acquired in the urban area of Shanghai, China, which were collected by a mobile survey vehicle for a single time at a relatively constant speed of approximately 30 km/h, with a length of 33.1 km and a collection time of 116 min. The MLS collection route, which is located in typical urban areas, is shown in the middle of Fig. 9. There were two areas in which the problem was likely to occur, and the quality of the MLS road point cloud was unstable, as shown by the red box in Fig. 9. According to the photos in Fig. 9, the MLS data acquisition environment of Areas I and II was quite complex, containing dense trees, tall buildings, and large overpasses. In addition, there were mainly straight roads in Area I, while some curved roads were in Area II.

Fig. 10 shows the raw MLS road point cloud in Areas I and II, which accounts for the degraded data quality. There were high-rise and densely distributed buildings in Area I. This environment may make GNSS positioning difficult because the window glass of many buildings' exacerbates the multipath effect, resulting in an inaccurate MLS trajectory. The environment in Area II includes dense street trees with a large canopy and overpass covering roads, which may lead to long-term GNSS signal outages. The trajectory error continuously accumulates over time because the IMU estimates the position of the MLS platform in this environment as prone to drift errors.

Owing to the road environment of the areas, the captured MLS point cloud data showed accuracy inconsistency phenomena (such as distortion or malposition) both vertically and horizontally. Table I lists the characteristics of the experimental data, including six representative problematic scenes.

In this article, raw MLS point clouds were sliced into segments for computational efficiency, each with a length of approximately 100 m. Moreover, the point cloud coordinates of the east, north, and up acquired by the GNSS receiver were normalized to the local coordinates of each segment which can be easily achieved by Burse–Wolf model [35]. Specifically, the X-axis is
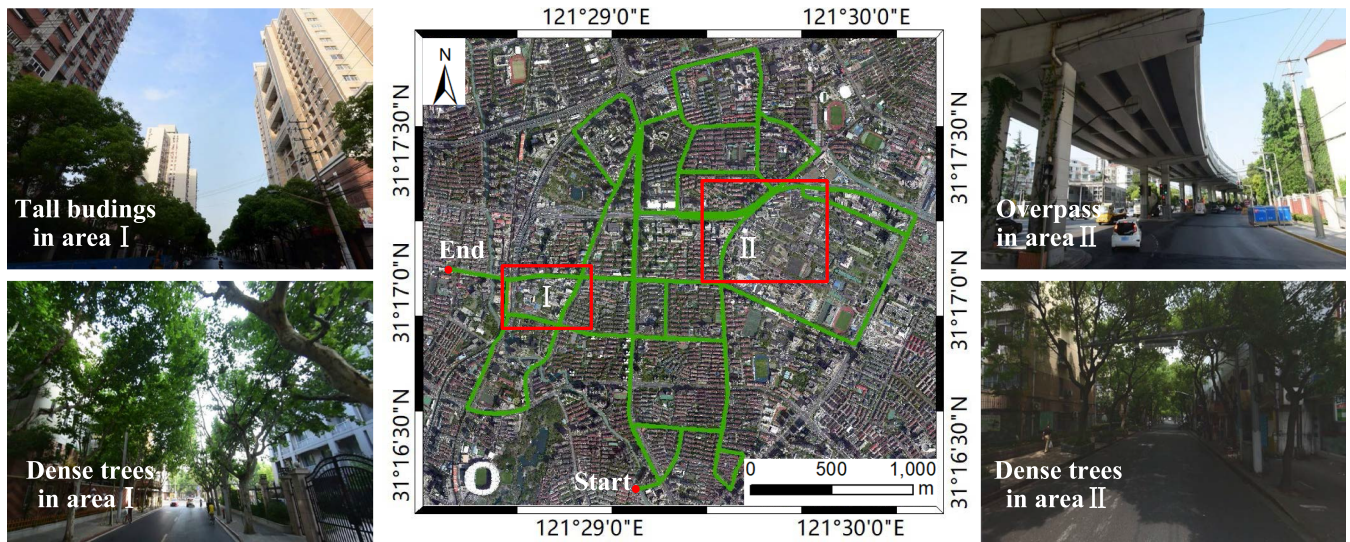
Fig. 9. MLS route plot and photos of typical scenes (the street photos are derived from Baidu Map).

TABLE I
CHARACTERISTICS OF EXPERIMENTAL DATA

Areas	Environment features	Problematic scenes	Problem description
Area I	Road surrounded by tall buildings	I-1	Slight horizontal and vertical distortions
		I-2	Vertical disjointed collapse
		I-3	Horizontal and vertical malpositions
Area II	Road covered by overpass and trees with large crown	II-1	Horizontal and vertical malpositions
		II-2	Horizontal and vertical malpositions
		II-3	Slight vertical subsidence

TABLE II
DETAILS OF MLS EMPLOYED FOR THE EXPERIMENTS

MLS system	Item	Value
Data acquisition sensor	Scan line amount	Single scan line
	Maximum range	920 m
	Minimum range	3 m
	Measuring accuracy	10 mm
	Field of view	330°
	update rate	10–200 Hz
Navigation sensor	GNSS	GPS, GLONASS, Galileo BeiDou
	Gyro bias instability of IMU	0.05°/h
	Orientation accuracy	Roll/Pitch: 0.005° Heading: 0.017°
	Position accuracy (GNSS available)	Horizontal: 0.01 m Vertical: 0.02 m

TABLE III
PARAMETERS IN THE EXPERIMENT FOR SCBCM

Name	Definition	Value
k_0	Threshold of baseline curvature	0.2 m^{-1}, for Scene I-1\I-2\I-3\ II-1\II-3 0.3 m^{-1}, for Scene II-2
s_0	Threshold of baseline gradient	0.1 %, for Scene I-1 and II-3 0.4 %, for Scene I-2\I-3\II-1\ II-2
l_c	Problematic field length	~25 m, determined by experiment
r	Neighborhood radius for curvature and gradient	0.3–0.5 m, related to point density

approximately along the road direction, which reduces the calculation error caused by excessively large coordinate values. In addition, point clouds around urban roads are removed to avoid the influence of ground objects such as buildings, vegetation, and traffic facilities. A cloth simulation filtering algorithm [36] filters the vehicles and pedestrians on the road surface, and the preprocessed point cloud data is shown in Fig. 11.

B. Data Collection

The experiments were conducted using a mobile laser-scanning system manufactured by CHCNAV (see Fig. 12), which has a vehicle-mounted laser scanner, IMU, and GNSS receiver. The details of the MLS employed for the experiments are listed in Table II. The accuracy of the MLS point cloud can reach the centimeter level when the GNSS signal is available. Each point captured by the MLS contains $\{x, y, z, \text{intensity}, \text{acquisition time}\}$, which are the geometry coordinates, intensity value, and time stamp, respectively.

C. Experimental Settings

Several parameters and their values used in the experiments are listed in Table III. Among these parameters, the threshold

of the baseline curvature and gradient is the prior knowledge according to the topography. The straighter and flatter the urban road, the smaller the k_0 and s_0 values should be. Therefore, we choose $k_0 = 0.2\,\text{m}^{-1}$ for nearly straight roads, and we increased it to $k_0 = 0.3\,\text{m}^{-1}$ for the curved road. It should be noted that some hilly topographies with natural slopes might have influenced the parameter setting of s_0. However, hilly topography
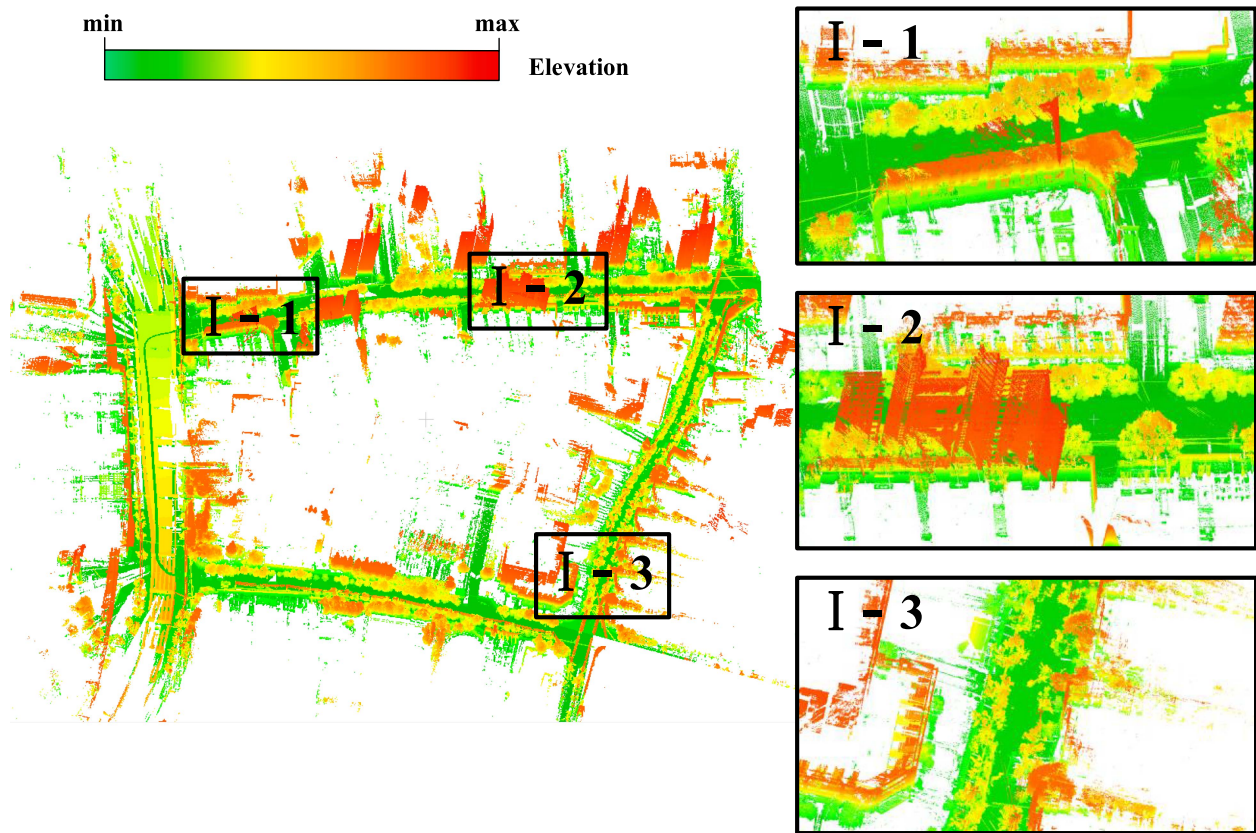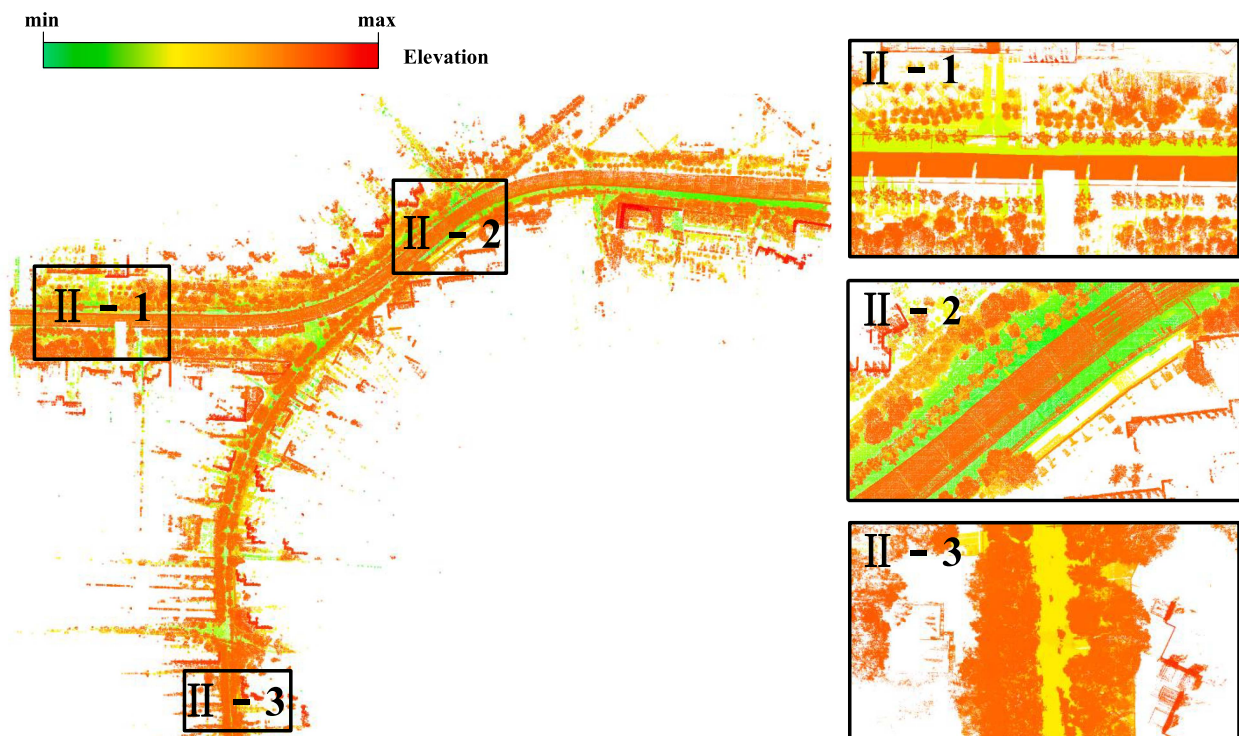
Fig. 10. (a) MLS point cloud of three problematic scenes in area I, colored by elevation. (b) MLS point cloud of three problematic scenes in area II, colored by elevation.
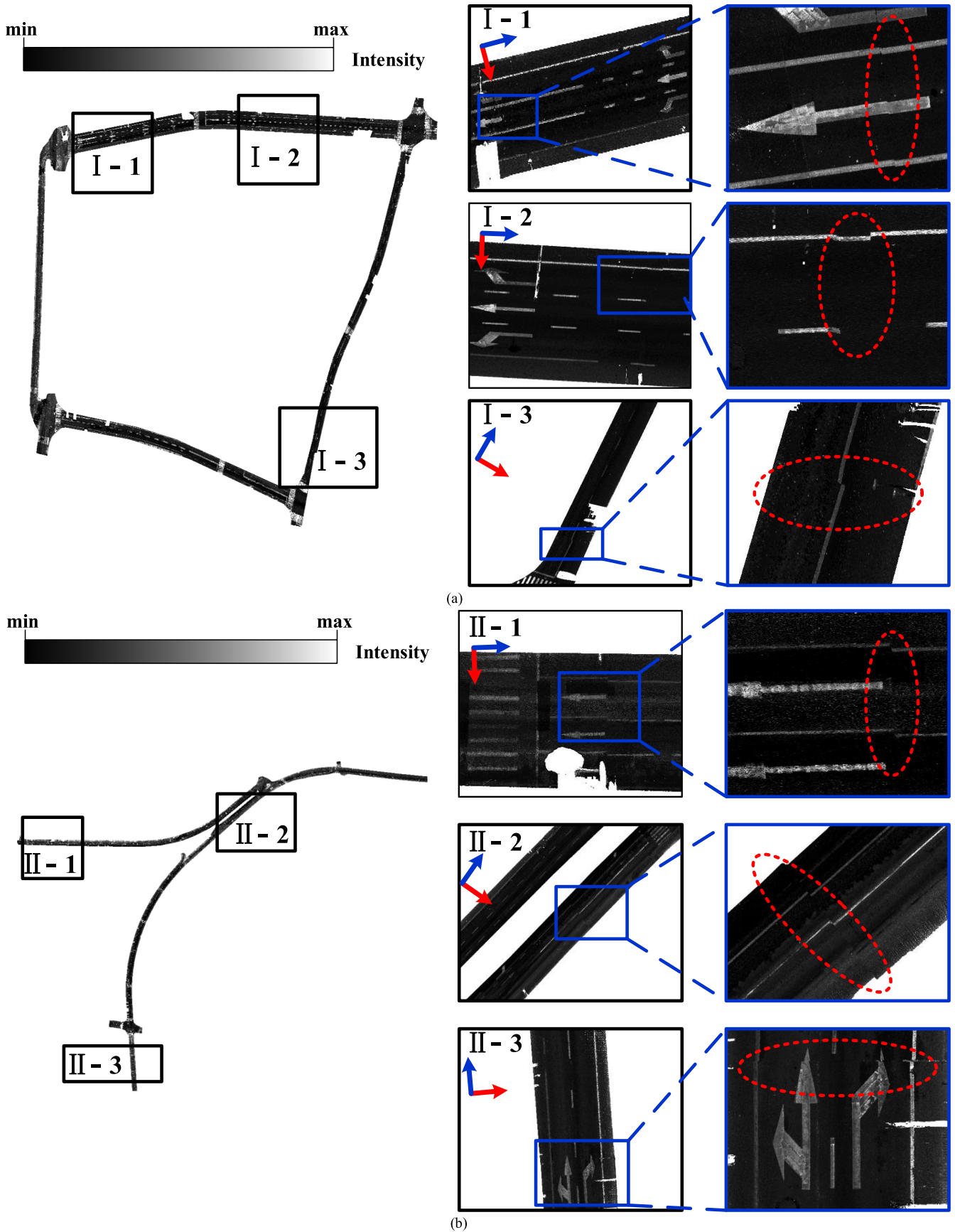
(a)

(b)

Fig. 11. (a) MLS point cloud of three problematic scenes in area I, colored by intensity. (b) MLS point cloud of three problematic scenes in area II, colored by intensity.

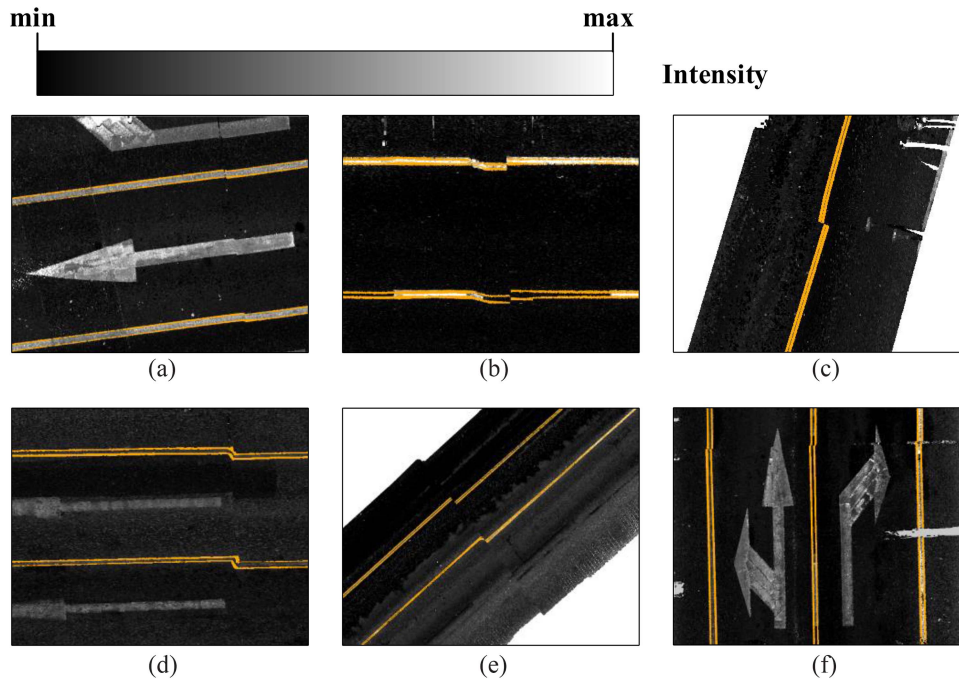Fig. 12.   Mobile laser scanning system.

Fig. 13.   Baseline generation for problematic scenes. (a)–(f) are results of baseline generation for the six problematic scenes, respectively.

is mainly located in spacious suburbs or rural areas, in which MLS can receive a robust GNSS signal, and the phenomenon of data accuracy inconsistency rarely arises. Therefore, we expect almost flat terrain (no sharp collapse and sinking) for urban areas; 0.1% and 0.4% are predefined for flat urban roads and urban roads with slight slopes.

l_c refers to length of problematic field, which is used to classify the feature points into corrective points. The longer the problem of inconsistency in MLS data accuracy persists, the larger l_c needs to be set. r refers to neighborhood radius for curvature and gradient. The more sparse the point cloud density, the larger r should be set to ensure accurate curvature and gradient. Meanwhile, larger value of neighborhood radius will consume more computational power and time, 0.5 is adapted to most of scenes.

With these parameters, the self-constrained condition of road point cloud baselines was constructed without additional reference information, and problematic data could be corrected accordingly.

D. Experimental Results of ScBCM

In this section, we present the results of the experiments described in the previous section, starting with the baseline generation of ScBCM. The baseline generation results of our approach are illustrated in Fig. 13 (yellow represents the baselines). The results show a significant inconsistency in the baselines' accuracy, which reflect the MLS data quality.

The ScBCM-corrected results of our approach and their impact on the point cloud are illustrated in Fig. 14, and the red
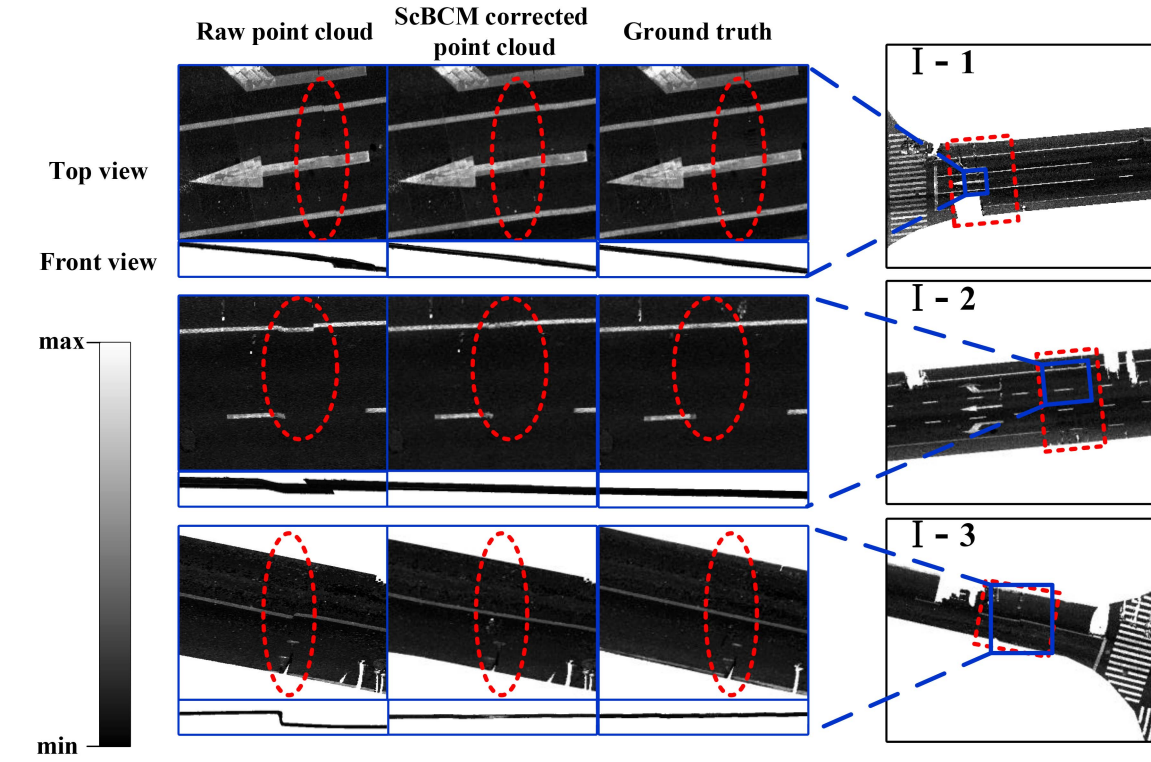
(a)
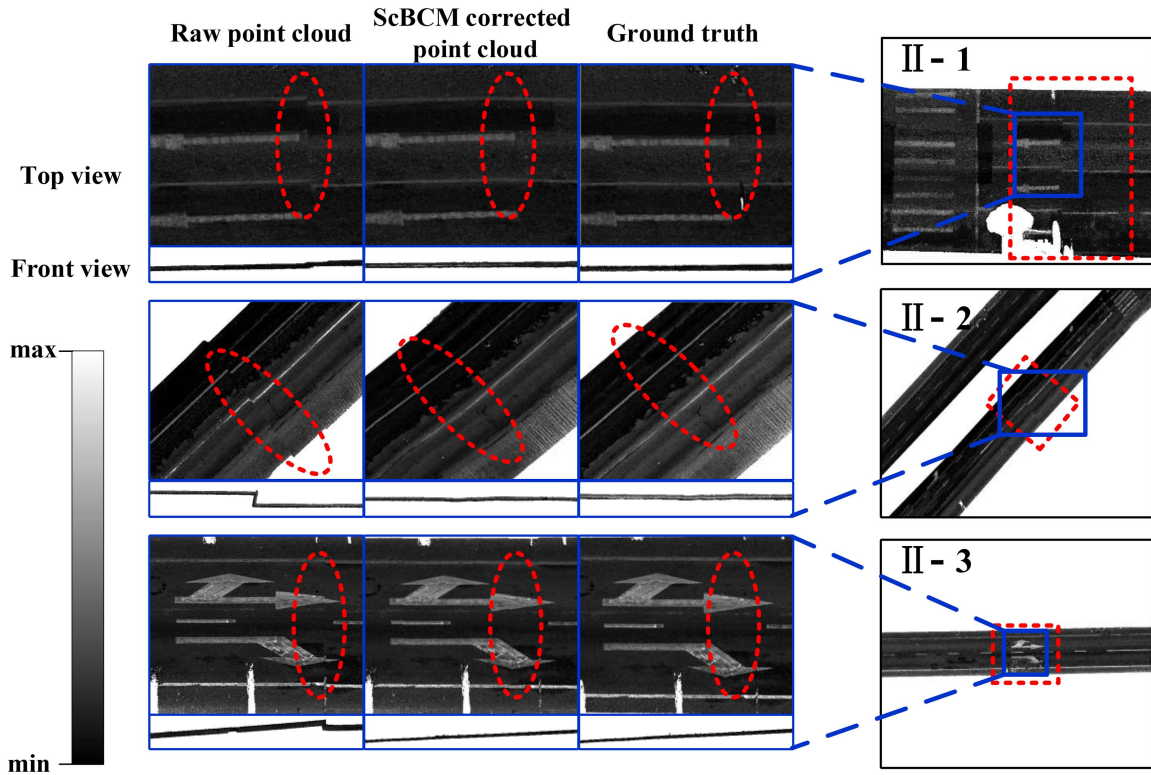
(b)

Fig. 14. (a) ScBCM results for three problematic scenes in area I. (b) ScBCM results for three problematic scenes in area II.
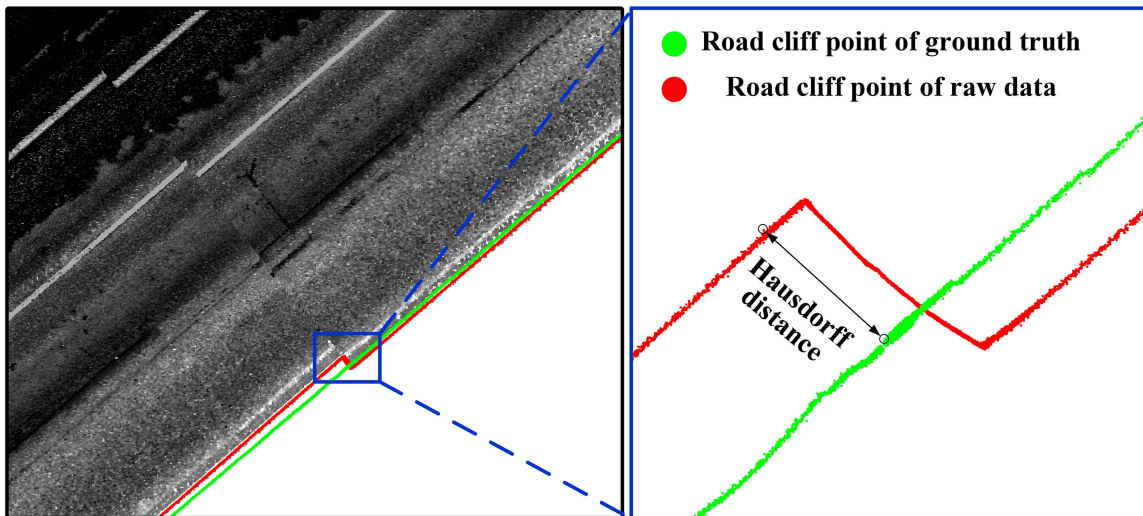
Fig. 15. Evaluation of road cliff points using Hausdorff distance.

dotted boxes indicate problematic region. The inconsistency in the accuracy of the MLS point cloud in a complex environment was significantly improved by the ScBCM. The vertical disjointed collapse and horizontal malposition are eliminated in the ScBCM-corrected results, the point clouds of which are closer to the ground truth given by the GCP-corrected point cloud. The results show that the proposed method can enhance the road point cloud's accuracy and consistency and improve the point cloud's quality after correction.

V. EVALUATION AND ANALYSIS

To assess the effectiveness of the ScBCM, a verification experiment for the correction processing of the point cloud was carried out. Subsequently, evaluation criteria were used to perform quantitative analysis and determine the optimal experimental settings.

A. Evaluation Criteria

Numerous GCPs were surveyed using RTK along the experimental MLS route to assess the proposed method's performance. The raw MLS data can be manually precorrected with GCPs using the Copre software suite. The precorrected MLS point clouds were saved as the ground truth to evaluate the accuracy and consistency of the experimental results. The accuracy of point cloud data corrected by control points was significantly higher than that of the point cloud data directly captured by MLS. Data consistency was reliable after intensive GCP-based precorrection, which met the requirements of urban road mapping.

After the ground truth was acquired and determined, the performance of the proposed method was evaluated using the Hausdorff distance, which expresses the dissimilarity between two point cloud sets. The Hausdorff distance of the point cloud

set $A = \{a^1, a^2, a^3, \ldots\}$ and $B = \{b^1, b^2, b^3, \ldots\}$ in Euclidean space can be calculated as follows [37]:

$$H(A, B) = \max\{h(A, B), h(B, A)\} \tag{18}$$

$$h(A, B) = \max_{a \in A} \min_{b \in B} \|a - b\| \tag{19}$$

$$h(B, A) = \max_{a \in A} \min_{b \in B} \|b - a\| \tag{20}$$

where $\|a - b\|$ represents the distance between Point Sets A and B.

To conduct experimental verification specifically, linear road cliff point clouds are selected from the ScBCM-corrected and ground truth point clouds accordingly. Their Hausdorff distance is the deviation compared to the ground truth, as shown in Fig. 15.

B. Accuracy Analysis for ScBCM Results

To verify the validity of the proposed method, linear road cliff point clouds were selected from the point clouds corrected by ScBCM and ground truth point clouds in six problematic scenes. The road cliff point cloud's scattered plots of the raw and corrected laser-scanning points are shown in Fig. 16, the red dotted boxes indicate problematic region. The blue dots are laser scanning points precorrected by GCPs, the laser scanning points from the raw MLS are shown by red crosses, and orange stars indicate the corresponding corrected laser scanning coordinates using ScBCM.

According to the results, the coordinates of the point cloud corrected by ScBCM (orange stars) are closer to those corrected by the GCPs (blue dots) than the raw laser ones (red crosses). This proves that the accuracy can be enhanced by the proposed method for the MLS data. Furthermore, according to the linear characteristics of the selected road cliff point cloud, the laser point cloud corrected by ScBCM eliminates noticeable distortion. It improves the quality of the MLS data vertically and horizontally.
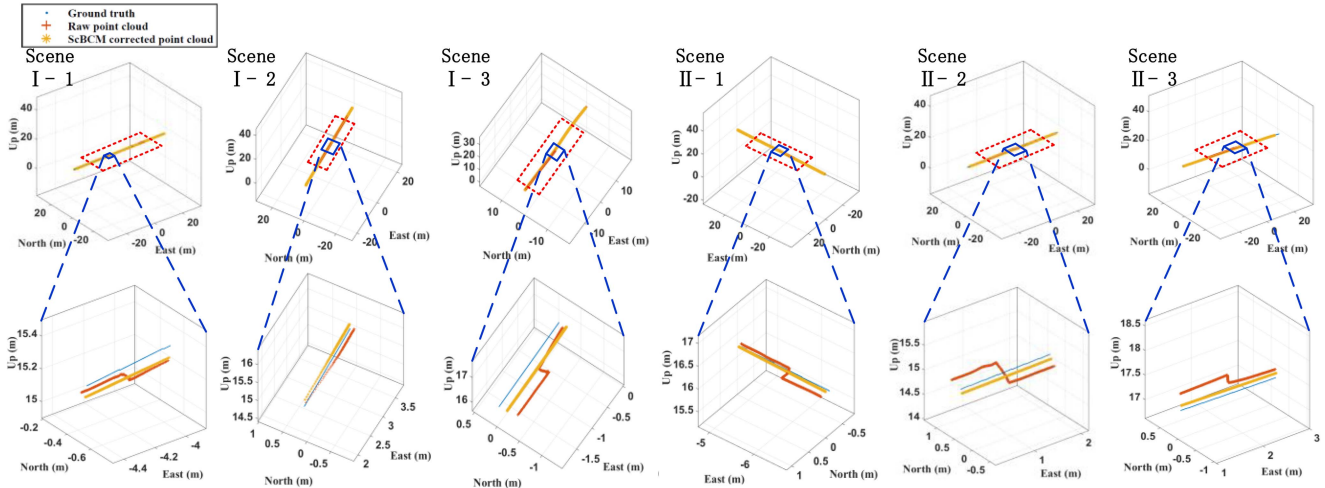
Fig. 16. Scatter plots of raw and corrected laser scanning points for six problematic scenes.

TABLE IV
DEVIATIONS OF RAW AND CORRECTED LASER SCANNING POINTS DATA USING ScBCM

Areas	Scenes	Deviations in 2D (dm)			Deviations in 3D (dm)		
		Before	After	Difference	Before	After	Difference
Area I	I-1	0.727	0.568	0.159	1.017	0.944	0.073
	I-2	1.491	0.333	1.158	1.623	0.742	0.881
	I-3	2.747	2.677	0.070	2.800	2.702	0.098
Area II	II-1	2.569	1.092	1.477	2.582	1.101	1.481
	II-2	2.737	0.874	1.863	2.811	0.908	1.903
	II-3	2.787	1.129	1.658	3.597	1.420	2.177
Average		2.176	1.112	1.064	2.405	1.303	1.102

In addition, the Hausdorff distance between the ScBCM-corrected point cloud and the GCP-corrected point cloud was calculated to quantitatively evaluate the problematic scenes' 3-D and 2-D data deviations, as shown in Table IV. The results show that the 3-D and 2-D average deviations of the ScBCM corrected point cloud are reduced by 1.10 and 1.06 dm, respectively. The results also verify that the self-constrained baseline method can effectively improve the accuracy of MLS point cloud data.

Although the deviation of corrected data has difficulties reaching the centimeter level because the data-driven correction approach faces limitations on the correction reference, only a few GCPs are needed for ScBCM-corrected data to further improve the data quality. This article can still significantly reduce the cost of manual labor for problematic MLS data, which avoids intensive GCPs surveyed in nonrigid deformation areas.

C. Accuracy Consistency Analysis for ScBCM Results

The linear road cliff point cloud in the problematic scenario was selected to further evaluate the accuracy and consistency of the ScBCM correction results. The curvature and gradient of the linear road cliff point cloud were calculated, as shown in Table V. Owing to traffic safety, urban road construction requires that the curvature and gradient of the road change gently. Considering that the selected linear road cliff point cloud has a short length, each scene should have a small standard deviation of the curvature and gradient.

The results in Table V show that the curvature and gradient of the MLS point cloud in the problematic scene exhibit significant and drastic changes before correction, particularly for Scenes I-3 and II-2. These drastic changes indicate that the MLS accuracy is inconsistent, resulting in poor quality in the six scenes. After the ScBCM correction, the standard deviation of the curvature and gradient in each problematic scene were significantly reduced, which is consistent with the road characteristics of gentle changes.
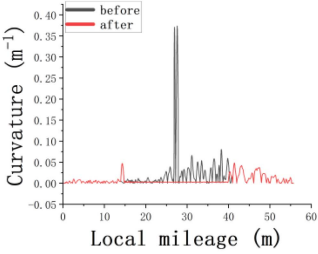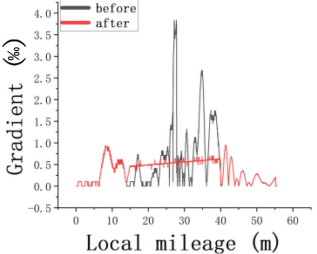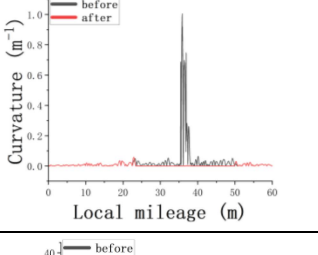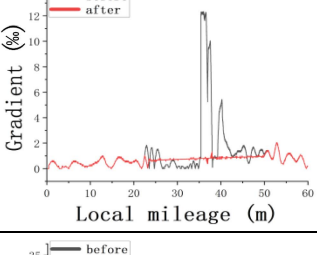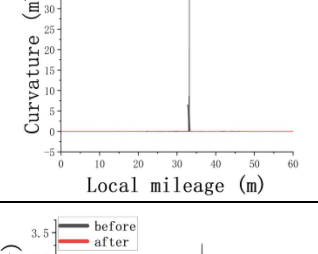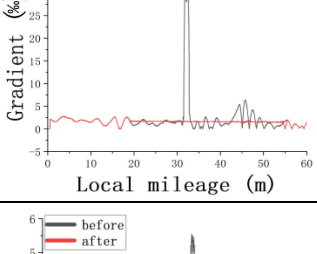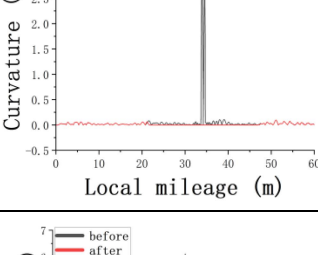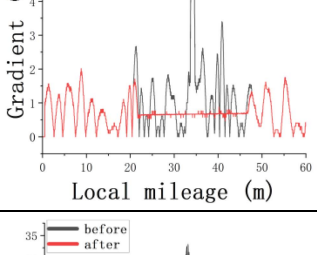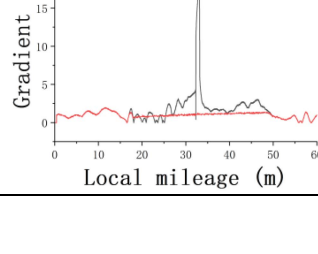
D. Impact of Problematic Field Length for ScBCM

Because the field length of problematic data determines the field of corrective points for nonrigid 3-D correction processing, the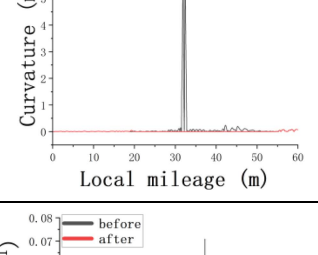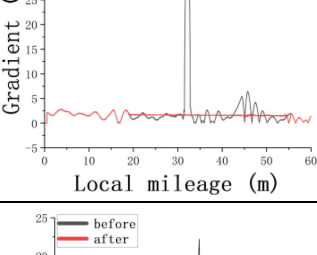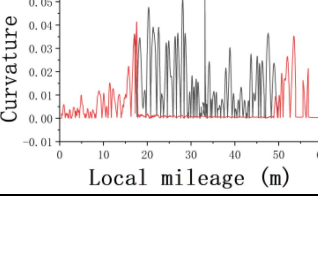 problematic field length l_c is one of the critical parameters for ScBCM. To explore the impact of the problematic field length l_c for ScBCM, we tested the value from 5 to 35 m with 5 m increments for l_c, while keeping other parameters fixed. Fig. 17 shows the results of the average deviation for problematic scenes using different field length values.

The results of the different l_c values demonstrate that all average deviations decreased in 2-D and 3-D after ScBCM processing. Note that the graph shows a significant decrease in 3-D, while the l_c value increased from 5 to 25 m. The main reason

TABLE V
CURVATURE AND GRADIENT OF RAW AND CORRECTED LASER SCANNING POINTS DATA USING SCBCM

| Scenes	Curvature information of road point cloud	Curvature standard deviation	Gradient information of road point cloud	Gradient standard deviation
I-1		Before: 0.041 After: 0.003		Before: 0.774 After: 0.266
I-2		Before: 0.367 After: 0.004		Before: 5.290 After: 0.194
I-3		Before: 2.367 After: 0.004		Before: 10.283 After: 0.379
II-1		Before: 0.374 After: 0.009		Before: 1.631 After: 0.294
II-2		Before: 1.202 After: 0.009		Before: 13.785 After: 0.280
II-3		Before: 0.006 After: 0.003		Before: 7.621 After: 0.201
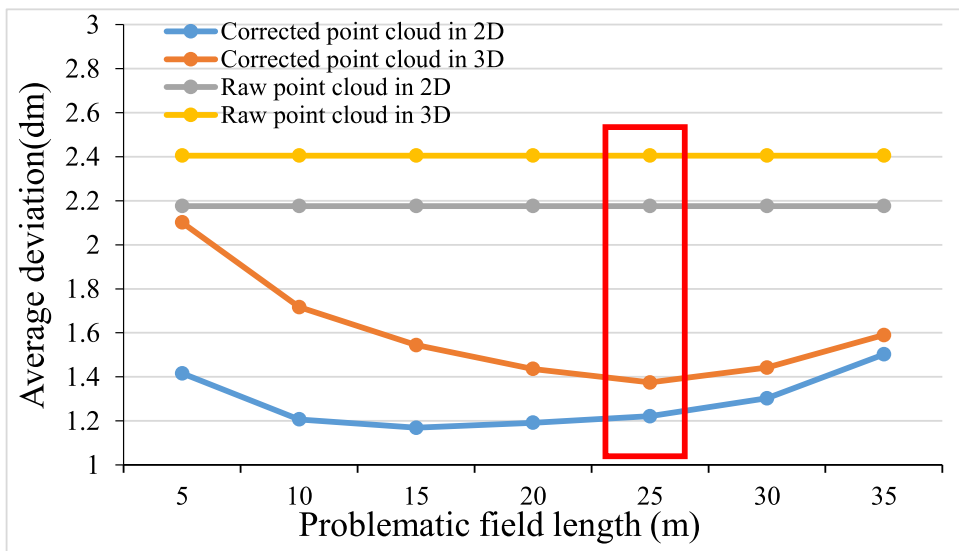
Fig. 17. Parameter influence of problematic field length for ScBCM in problematic scenes.
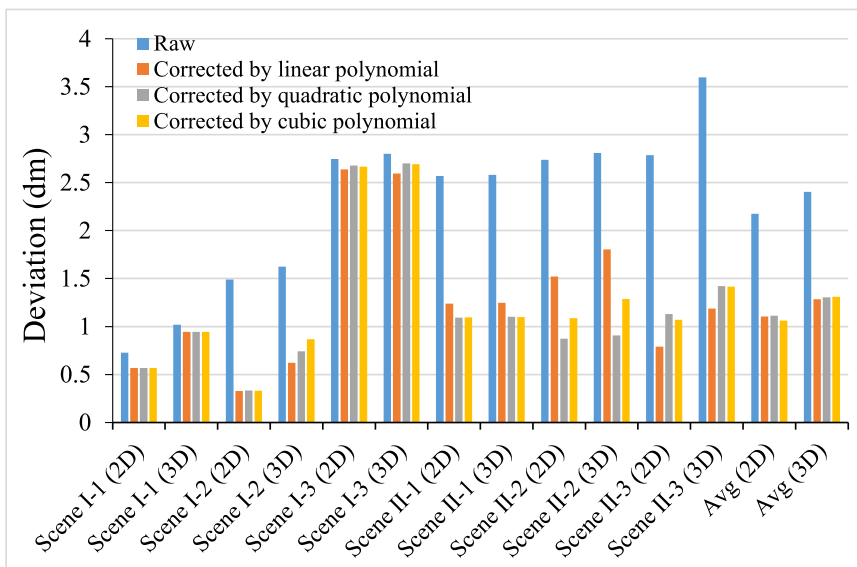

Fig. 18. Influence of different baseline expressions for ScBCM.

for this is that some slightly problematic data may be divided into reference points when l_c is set as a small value. The 3-D deviations show an upward trend when the l_c value is greater than 25 m, which is probably because the reference point is far away from the problem location, reducing the self-constraint ability of the baselines, while a large l_c value is applied. The best value of the problematic field length was determined at $l_c = 25$ m, as shown in the red box of Fig. 17 because the average deviation at $l_c = 25$ m is the best result in 3-D and acceptable in 2-D.

E. Impact of Baseline Expression for ScBCM

With the optimal parameters, the performance of the proposed ScBCM was further evaluated to check its robustness to different baseline expressions, including linear, quadratic, and cubic

polynomial fitting. Fig. 18 summarizes the 2-D and 3-D results for the problematic scenes.

According to the 2-D deviation of different baseline expressions in Fig. 18, the deviation of the quadratic polynomial is smaller than that of the others in Scene II-2, potentially because the baseline expression of the quadratic polynomial is more adaptable to curved roads. The 2-D deviation of most scene data corrected by linear polynomials is the best for straight roads, except Scene II-1. As for Scene II-1, though the quadratic polynomial results are a little bit better, the 2-D deviation of quadratic polynomial corrected data is very close to one of the linear polynomial corrected data. The reason might be that the vertex of the curved reference line expressed by the quadratic polynomial is closer to the ground truth, even though the reference line should be straight for straight roads. This effect can be effectively weakened by introducing a few GCPs for the point

cloud already corrected by ScBCM, to further acquire higher data quality.

In addition, most deviations of 2-D are similar to the results of 3-D, the reason for which might be that the slope is gentle in urban terrain. Compared to the raw point cloud in Fig. 18, all the point cloud deviations of the different baseline expressions corrected by ScBCM are significantly reduced. The results indicate that the proposed ScBCM provides a corrected point cloud with less deviation, achieving the desired comprehensive performance regardless of baseline expression and dimensions.

VI. Discussion

A. Applicability of the Proposed Method

This research's method can be applied to roads with different curvature conditions, regardless of whether the road is straight or curve, because the reference line is constructed by polynomials for nonrigid correction. Besides, snakes are active contour models guided by external constraint forces and influenced by image forces, they can lock on nearby edges and locate them accurately, and thus the baseline generation method in this article can be applied to problem scenes with distortions. However, it should be noted that different topographies might affect the performance of the proposed method. For example, some hilly topography might have natural slopes, influencing the parameter setting. However, hilly topography is mainly located in spacious suburbs or rural areas, in which MLS can receive a robust GNSS signal, and the phenomenon of data accuracy inconsistency rarely arises. Therefore, we expect a nearly flat terrain for experimental scenes to apply hilly topography in urban areas.

Regarding hilly topography in urban areas, road construction and marking with paints are designed according to certain technical standards because of the safety of urban traffic. This implies that the gradient of most roads changes moderately to ensure traffic safety, even in the hilly topography of urban areas. This gentle gradient change significantly differs from the drastic gradient change in problematic data. Consequently, our method theoretically applies to hilly urban areas, where the process is similar to the flat terrain investigated here. The key requirement for ScBCM is parameter setting; fortunately, it can be done by referring to some technical standards for road construction (e.g., Technical Standard of Highway Engineering JTG B01-2014 in China).

B. Uncertainty in Baselines

The quality of baseline generation is crucial to the reliability of the proposed 3-D correction model. In reality, however, it is impractical to perfectly extract road markings to generate baselines because symbolic road markings (such as arrows) and some worn road markings are difficult to use for baseline generation. A practical strategy is to extract solid or dotted road markings, the feature of which is more robust information, and use multiple road markings for the correction model to reduce the impact of single-worn road markings, as in this article. However, the influence of wear on the marking extraction cannot be completely eliminated. In other words, some baselines cannot perfectly reflect the data quality of the MLS point cloud. In future article, developing a more comprehensive strategy for baseline selection and reducing the uncertainty introduced by baseline generation will be necessary.

Concerning the baselines generated by road markings, ensuring that the extracted road markings correctly reflect the problematic point cloud is critical. Road markings are designed and painted according to specifications, and adjacent road markings have similar spatial structures; the left and right road markings on the same lane are in the same direction. Thus, the more similar the structure of the extracted adjacent road markings in the same lane, the better the quality of the generated baselines. Developing effective metrics (e.g., structural similarity of adjacent baselines) to identify useful baselines would be interesting.

C. Other Choices of Baselines Generation

In this article, road markings were used to generate baselines. It would be interesting to examine whether other baseline generation choices (e.g., curbside) are suitable for an ScBCM. This can be an important consideration when there are no effective road markings owing to newly constructed or dilapidated roads. Hence, effective road markings may not be painted promptly, or large wear may exist. However, much curbside is designed and built according to some specifications, providing feature information of the road point cloud. These curbsides can help generate baselines when road markings are struggling to be extracted. Therefore, it is worthwhile to develop solutions to fill the gaps introduced by the lack of road markings, maximize these data, and distill useful feature information for baseline generation.

VII. Conclusion

We developed a self-constrained baseline 3-D correction approach for MLS point clouds in a complex urban road environment. Instead of directly correcting inaccurate MLS platform positions, the proposed method extracts intrinsic road characteristics from raw MLS. Hence, it enhances the data accuracy consistency without additional reference information, which effectively improves the quality of the urban road point cloud. The main contributions of the proposed approach are as follows:

1) Baselines of MLS point clouds are proposed to reflect data accuracy inconsistency quantificationally in areas where MLS positioning is inaccurate owing to the loss of the GNSS signal, which can effectively locate problematic MLS data vertically and horizontally.
2) An ScBCM is designed according to the intrinsic characteristics of road information extracted from raw point clouds and nonrigid correction processing. The ScBCM is devised to correct the MLS point cloud to the same accuracy level, especially in a complex environment.
3) The proposed method's performance evaluation and analysis are demonstrated for six experimental scenarios. The experimental results showed that the 3-D average deviation of problematic data was reduced by 1.10 dm, demonstrating that ScBCM significantly improved the quality of the MLS point cloud.

Although this article is satisfactory for most roads, the model parameters can be further optimized to meet the higher-precision data requirements. Therefore, future article will focus on developing more detailed processing steps to adjust the model parameters adaptively according to the scene. In addition, more advanced road marking algorithms may be integrated and applied to ScBCM in future article to improve performance.

REFERENCES

[1] Y. Wang et al., "A survey of mobile laser scanning applications and key techniques over urban areas," *Remote Sens.*, vol. 11, no. 13, pp. 1–20, Jul. 2019.

[2] A. Kukko et al., "Multiplatform mobile laser scanning: Usability and performance," *Sensors*, vol. 12, no. 9, pp. 11712–11733, Sep. 2012.

[3] K. Chen et al., "Automatic building information model reconstruction in high-density urban areas: Augmenting multi-source data with architectural knowledge," *Automat. Construction*, vol. 93, pp. 22–34, Sep. 2018.

[4] H. Guan et al., "Use of mobile LiDAR in road information inventory: A review," *Int. J. Image Data Fusion*, vol. 7, no. 3, pp. 219–242, 2016.

[5] W. Xiao et al., "Street-side vehicle detection, classification and change detection using mobile laser scanning data," *ISPRS J. Photogramm. Remote Sens.*, vol. 114, pp. 166–178, Apr. 2016.

[6] J. Balado et al., "Multi feature-rich synthetic colour to improve human visual perception of point clouds," *ISPRS J. Photogramm. Remote Sens.*, vol. 196, pp. 514–527, Feb. 2023.

[7] Y. Chen et al., "Feasibility study of using mobile laser scanning point cloud data for GNSS line of sight analysis," *Mobile Inf. Syst.*, vol. 2017, 2017, Art. no. 5407605.

[8] J.-Y. Han, C.-S. Chen, and C.-T. Lo, "Time-variant registration of point clouds acquired by a mobile mapping system," *IEEE Geosci. Remote Sens. Lett.*, vol. 11, no. 1, pp. 196–199, Jan. 2014.

[9] P. Schaer and J. Vallet, "Trajectory adjustment of mobile laser scan data in GPS denied environments," *Int. Arch. Photogramm. Remote Sens. Spatial Inf. Sci.*, vol. XL-3/W4, pp. 61–64, Feb. 2016.

[10] H. Jing et al., "Efficient point cloud corrections for mobile monitoring applications using road/rail-side infrastructure," *Surv. Rev.*, vol. 53, no. 378, pp. 235–251, May 2021.

[11] W. Liu, Z. Li, Y. Li, S. Sun, and M. A. Sotelo, "Using weighted total least squares and 3-D conformal coordinate transformation to improve the accuracy of mobile laser scanning," *IEEE Trans. Geosci. Remote Sens.*, vol. 58, no. 1, pp. 203–217, Jan. 2020.

[12] Y. Gao et al., "Automatic geo-referencing mobile laser scanning data to UAV images," *Int. Arch. Photogramm., Remote Sens. Spatial Inf. Sci.*, vol. XL-1/W4, pp. 41–46, Aug. 2015.

[13] X. Zou, "Mobile laser point cloud position consistency correction in urban scene," M.S. thesis, Dept. School Geodesy Geomatics, Wuhan Univ., Wuhan, China, 2019.

[14] Z. Hussnain, S. O. Elberink, and G. Vosselman, "Enhanced trajectory estimation of mobile laser scanners using aerial images," *ISPRS J. Photogramm. Remote Sens.*, vol. 173, pp. 66–78, Mar. 2021.

[15] Z. Hussnain, S. O. Elberink, and G. Vosselman, "Automatic extraction of accurate 3D tie points for trajectory adjustment of mobile laser scanners using aerial imagery," *ISPRS J. Photogramm. Remote Sens.*, vol. 154, pp. 41–58, Aug. 2019.

[16] M. Javanmardi et al., "Towards high-definition 3D urban mapping: Road feature-based registration of mobile mapping systems and aerial imagery," *Remote Sens.*, vol. 9, no. 10, Oct. 2017, Art. no. 975.

[17] C. Toth et al., "Terrain-based navigation: A tool to improve navigation and feature extraction performance of moblie mapping systems," *Boletim De Ciencias Geodesicas*, vol. 15, no. 5, pp. 807–823, 2009.

[18] M. Zhong et al., "Recovering missing trajectory data for mobile laser scanning systems," *Remote Sens.*, vol. 12, no. 6, pp. 1–21, Mar. 2020.

[19] F. Yu, J. Xiao, and T. Funkhouser, "Semantic alignment of LiDAR data at city scale," in *Proc. IEEE Conf. Comput. Vis. Pattern Recognit.*, 2015, pp. 1722–1731.

[20] T. Shiratori et al., "Efficient large-scale point cloud registration using loop closures," in *Proc. Int. Conf. 3D Vis.*, 2015, pp. 232–240.

[21] B. Yang et al., "A marker-free calibration method for mobile laser scanning point clouds correction," *Int. Arch. Photogramm., Remote Sens. Spatial Inf. Sci.*, vol. XLIII-B2-2020, pp. 347–354, 2020.

[22] L. Ma et al., "Mobile laser scanned point-clouds for road object detection and extraction: A review," *Remote Sens.*, vol. 10, no. 10, pp. 1–33, Oct. 2018.

[23] X. Mi et al., "A two-stage approach for road marking extraction and modeling using MLS point clouds," *ISPRS J. Photogramm. Remote Sens.*, vol. 180, pp. 255–268, Oct. 2021.

[24] C. Wen et al., "A deep learning framework for road marking extraction, classification and completion from mobile laser scanning point clouds," *ISPRS J. Photogramm. Remote Sens.*, vol. 147, pp. 178–192, Jan. 2019.

[25] R. Yang et al., "Accurate road marking detection from noisy point clouds acquired by low-cost mobile LiDAR systems," *ISPRS Int. J. Geo-Inf.*, vol. 9, no. 10, pp. 1–14, Oct. 2020.

[26] S. Chen, Z. Zhang, R. Zhong, L. Zhang, H. Ma, and L. Liu, "A dense feature pyramid network-based deep learning model for road marking instance segmentation using MLS point clouds," *IEEE Trans. Geosci. Remote Sens.*, vol. 59, no. 1, pp. 784–800, Jan. 2021.

[27] M. Yang et al., "Laser data based automatic recognition and maintenance of road markings from MLS system," *Opt. Laser Technol.*, vol. 107, pp. 192–203, Nov. 2018.

[28] L. Fang et al., "A graph attention network for road marking classification from mobile LiDAR point clouds," *Int. J. Appl. Earth Observ. Geoinf.*, vol. 108, Apr. 2022, Art. no. 102735.

[29] M. Cheng, H. Zhang, C. Wang, and J. Li, "Extraction and classification of road markings using mobile laser scanning point clouds," *IEEE J. Sel. Topics Appl. Earth Observ. Remote Sens.*, vol. 10, no. 3, pp. 1182–1196, Mar. 2017.

[30] T. Pun, "A new method for gray-level picture thresholding using the entropy of the histogram," *Signal Process.*, vol. 2, no. 3, pp. 223–237, 1980.

[31] M. Kass, A. Witkin, and D. Terzopoulos, "SNAKES – active contour models," *Int. J. Comput. Vis.*, vol. 1, no. 4, pp. 321–331, 1987.

[32] B. Riveiro et al., "Automatic detection of zebra crossings from mobile LiDAR data," *Opt. Laser Technol.*, vol. 70, pp. 63–70, Jul. 2015.

[33] W. Luo and L. Li, "Automatic geometry measurement for curved ramps using inertial measurement unit and 3D LiDAR system," *Automat. Construction*, vol. 94, pp. 214–232, Oct. 2018.

[34] J. K. Shrestha et al., "A multi-objective analysis of a rural road network problem in the hilly regions of Nepal," *Transp. Res. Part A-Policy Pract.*, vol. 64, pp. 43–53, Jun. 2014.

[35] R. Deakin, "A note on the Bursa–Wolf and Molodensky–Badekas transformations," School of Mathematical and Geospatial Sciences, RMIT University, 1, 21, 2006.

[36] W. Zhang et al., "An easy-to-use airborne LiDAR data filtering method based on cloth simulation," *Remote Sens.*, vol. 8, no. 6, pp. 1–22, Jun. 2016.

[37] D. P. Huttenlocher, G. A. Klanderman, and W. J. Rucklidge, "Comparing images using the Hausdorff distance," *IEEE Trans. Pattern Anal. Mach. Intell.*, vol. 15, no. 9, pp. 850–863, Sep. 1993.

Youyuan Li received the B.S. degree in surveying and geoinformatics from the Shandong University of Science and Technology, Qingdao, China, in 2016. He is currently working toward the M.S. degree in visual-aid data enhancement technology of point cloud for road scenes with the College of Surveying and Geo-Informatics, Tongji University, Shanghai, China.

His research interests include LiDAR data processing and mobile mapping.

Chun Liu received the B.S. and M.S. degrees in surveying and geoinformatics from the Shandong University of Science and Technology, Qingdao, China, in 1995 and 1998, respectively, and the Ph.D. degree in surveying and geoinformatics from the Tongji University, Shanghai, China, in 2000.

He is currently a Full Professor with the College of Surveying and Geo-Informatics, Tongji University. His research interests include complex realistic scene semantic cognition and modeling.

Yuanfan Qi received the B.S. degree in surveying and geoinformatics from the Tongji University, Shanghai, China, in 2016. He is currently working toward the Ph.D. degree in generalized point cloud driven intelligent driving perception enhancement in complex traffic scenarios with the College of Surveying and Geo-Informatics, Tongji University.

His research interests include LiDAR data processing and mobile mapping.

Hangbin Wu received the B.S. and Ph.D. degrees in surveying and geoinformatics from the Tongji University, Shanghai, China, in 2005 and 2010, respectively.

He is currently an Associate Professor with the College of Surveying and Geo-Informatics, Tongji University. His research interests include LiDAR data processing and trajectory data mining.